Global Energy Interconnection 9 (2026) 186–207

KeAi
CHINESE ROOTS
GLOBAL IMPACT

Global Energy Interconnection
Development and Cooperation Organization

Global Energy Interconnection

Contents lists available at ScienceDirect
journal homepage: www.elsevier.com/locate/gloei

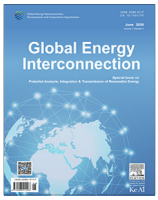

Research on cooperative operation optimization of Nash-Stackelberg game in multiple virtual power plants under multiple uncertainties

Lei Dong [a,*], Shuaibo Zhang [a], Yang Li [b], Zibo Wang [b], Binwen Zhang [b], Hong Zhu [c], Wenlu Ji [c]

[a] School of Electric Engineering, North China Electric Power University, Changping District, Beijing 102206, PR China
[b] China Electric Power Research Institute, Haidian District, Beijing 100192, PR China
[c] State Grid Jiangsu Electric Power Co., LTD. Nanjing Power Supply Branch, Jiangsu Province, Nanjing 210019, PR China

Received 15 June 2025; revised 22 October 2025; accepted 27 October 2025

Abstract

This paper suggests a way to improve teamwork and reduce uncertainties in operations by using a game theory approach involving multiple virtual power plants (VPP). A generalized credibility-based fuzzy chance constraint programming approach is adopted to address uncertainties stemming from renewable generation and load demand within individual VPPs, while robust optimization techniques manage electricity and thermal price volatilities. Building upon this foundation, a hierarchical Nash-Stackelberg game model is established across multiple VPPs. Within each VPP, a Stackelberg game resolves the strategic interaction between the operator and photovoltaic prosumers (PVP). Among VPPs, a cooperative Nash bargaining model coordinates alliance formation. The problem is decomposed into two subproblems: maximizing coalitional benefits, and allocating cooperative surpluses via payment bargaining, solved distributively using the alternating direction method of multipliers (ADMM). Case studies demonstrate that the proposed strategy significantly enhances the economic efficiency and uncertainty resilience of multi-VPP alliances.

Keywords: Virtual power plant; Fuzzy chance constraint; Generalized credibility; Robust optimization; Nash-Stackelberg game; Nash Bargaining

0 Introduction

In the context of global energy decentralization and multi-energy complementarity, virtual power plants (VPP) are pivotal in enhancing the efficient exploitation of distributed energy [1]. The influence of uncertainty factors, including the variability of renewable energy production and frequent market price fluctuations, is progressively complicating the multi-agent collaborative management of VPPs. Consequently, achieving multi-agent collaborative operation in an unpredictable environment is of considerable importance [2].

With the large-scale integration of distributed resources (e.g., new energy generation units, energy storage, controllable loads), multiple operational entities have emerged in VPPs. These entities differ in optimization goals and face information asymmetry, making it essential to clarify the coordination mechanisms within a single VPP and across multiple VPPs, as well as establish an efficient operation framework. Game theory effectively facilitates the coordination of interest equilibrium across various actors and has increasingly been utilized in the synchronized operation of VPPs in recent years. Comprising two categories:

Peer review under the responsibility of Global Energy Interconnection Group Co. Ltd.
* Corresponding author.
E-mail address: donglei@ncepu.edu.cn (L. Dong).

https://doi.org/10.1016/j.gloei.2025.10.005

non-cooperative games and cooperative games. Non-cooperative games are exemplified by the Stackelberg game [3]. Reference [4] formulates a Stackelberg game model to examine the non-cooperative dynamics between the upper-level distribution network operator and the lower-level VPP. Reference [5] constructed a two-layer Stackelberg game model between EH and users, achieving the integration of the game framework and uncertainty modeling. The leader–follower game is also often used to formulate the optimal pricing strategy and guide user behavior. In the leader–follower game framework of Reference [6], the aggregator of producers and consumers acts as the leader, dynamically formulating coupled electricity prices and carbon prices, while the producers and consumers as followers adjust their own electricity usage behavior to reduce costs and carbon emissions. References [4–6] attain reciprocal responses inside the system, enhancing their own objectives. Non-cooperative games prioritize individual interests; Yet, their disregard for collective interests may result in a socially suboptimal outcome. Cooperative games emphasize collective advantages. In the context of collaborative optimization across numerous VPPs, global resource sharing and coordinated optimization can be attained, typically depicted as coalition games [7] or Nash bargaining models [8]. Reference [9] developed a cooperative game model utilizing Nash bargaining between solar power generation and power-to-hydrogen, to optimize the benefits of the cooperative alliance. The previously mentioned cooperative game model offers substantial benefits in attaining optimal overall advantages for the alliance and equitable profit distribution. Nonetheless, while safeguarding the alliance's overall optimal advantage, it remains essential to further examine the relational dynamics among the members inside the alliance. Reference [10] created a mixed game architecture with an upper layer featuring a Stackelberg game between the VPP and the RIES alliance, and a lower layer consisting of a cooperative game among the members of the RIES alliance. Reference [11] establishes a leader–follower game among the upper-level power grid, gas grid, and lower-level energy stations. Subsequently, a Nash cooperative game is subsequently formulated between the upper-level distribution and gas networks. The Nash-Stackelberg game (N-S game) framework, as delineated in references [10,11] and this paper, amalgamates the benefits of master–slave and cooperative games, thereby ensuring the stable operation of VPPs while accounting for the competitive and cooperative dynamics among diverse entities, thus offering a more lucid depiction of the interaction processes among these entities. To protect the privacy of the participants in the game, distributed algorithms are often used for solution. Currently, there have been studies that apply distributed algorithms to the game framework: Literature [12] uses the binary method to handle the Stackelberg game model, but it is mainly applicable to single-variable problem scenes and is difficult to deal with the optimization problems of coupled interactions among multiple entities. The goal cascading method focuses on handling game optimization problems with clear hierarchical structures [13]. However, the three VPP entities studied in this paper have a horizontal parallel structure and need to handle multiple coupled variables such as interaction power and interaction price. Therefore, compared with the binary method and the goal cascading method, the Alternating direction method of multipliers (ADMM) is more suitable for solving the N-S game model among multiple VPPs, and shows good convergence in the multi-entity distributed optimization scene. Meanwhile, the game models presented in the aforementioned literature are predominantly constructed under ideal conditions, neglecting the stochastic nature of renewable energy output, market price volatility, and other pertinent factors. This may result in unforeseen differences in the strategy payoffs encountered by participants during the game, impacting the stability and efficacy of decision-making.

In the operation of VPPs, as the number of unknown variables escalates, it is imperative to further assess the influence of these uncertainties during the operational process to guarantee the system's safe, dependable, and affordable functioning. The primary techniques for modeling uncertainty are stochastic optimization [14] and robust optimization [15,16]. Reference [17] introduces opportunity constraints and uses cooperative game theory to achieve multi time scale collaborative optimization of multiple VPPs. Reference [18] adopts interval modeling combined with robust optimization to deal with the uncertainty of new energy, and combines cooperative game theory to enhance the overall economic benefits of the alliance. References [19,20] employ robust optimization techniques to tackle the dual uncertainties of carbon pricing and renewable energy production, integrating game theory for optimal scheduling. The cited literature optimizes VPP operations using game theory models while addressing uncertainties to achieve optimal strategies under uncertainty. However, it fails to distinguish between different types of uncertain variables, often overlooks the dynamic characteristics of the source-load side in uncertainty modeling, and typically adopts a uniform constraint confidence level or accounts for uncertainty across all scheduling periods—failing to accurately reflect how varying time-interval risk levels influence strategies.

This work formulates a Nash-Stackelberg game operational optimization model to improve the collaborative operational capacity of various VPPs amidst uncertainties. The comparison between the work presented in this paper and the previous references is shown in Table 1. The primary contributions are: A Nash-Stackelberg game framework for cooperative operational optimization of many VPPs under various uncertainty is devised. This entails developing a Stackelberg game framework between virtual

Table 1
Comparison of existing literature models.

Ref.	Game model		Uncertainty Model	
	Stackelberg	Nash	Source and load	Price
[6]	√	×	√	×
[16,17]	×	√	√	×
[19,20]	×	×	√	√
[23]	×	√	√	√
Article	√	√	√	√

power plant operator (VPPO) and photovoltaic prosumers (PVP), as well as formulating a Nash cooperative game model among various VPP entities. Instead, fuzzy chance constraints are adopted, and trapezoidal fuzzy sets are constructed to handle source-load side uncertainties. Through equivalence clarification, differentiated modeling of fuzzy events with different risk preferences is realized based on generalized believability.

The structure of the remaining part of this article is as follows: Section 1 constructs the VPP operation framework and the main model; Section 2 conducts multiple uncertainty modeling; Section 3 establishes the Nash-Stackelberg game model; Section 4 verifies the model's validity through multiple scene examples; Section 5 summarizes the research conclusions and looks forward to future work.

1 VPP Nash-Stackelberg game operation optimization model

1.1 VPP collaborative operation framework

The VPP system includes the VPPO and the PVP. The operation framework of the Nash-Stackelberg game is shown in Fig. 1.

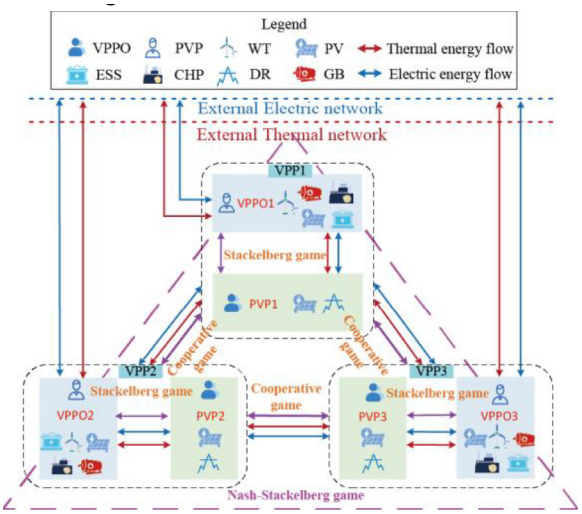

Fig. 1. The Nash-Stackelberg game framework.

The Nash-Stackelberg game framework comprises two components: the Stackelberg game model between VPPO and PVP, and the cooperative game model among VPPs. In the primary-slave game component, the VPP operator, acting as the leader, establishes dynamic electricity and thermal pricing for the subordinate solar prosumer. Upon responding to the prices, the PVP execute demand responses and relay their energy purchase requirements to the higher-level operator. Upon receiving the energy procurement requests from the prosumer, the VPP operator modifies the output of the units to minimize its operational expenses. Preserve the system's energy supply. In the cooperative segment of the game, each VPP engages in peer-to-peer (P2P) exchanges of electrical and thermal energy with other VPP entities, while preserving internal autonomy, so constituting a cohesive VPP cooperative alliance. The optimization of cooperative advantages and the allocation of benefits within the VPP alliance are accomplished via Nash bargaining.

1.2 VPP operator model

The VPPO contains combined thermal and power unit, new energy power generation units and electric energy storage devices internally. As a leader, it sells electricity and thermal energy to followers and prosumer by setting dynamic electricity and thermal prices to achieve optimal economic operation. Its objective function model is:

$$\begin{aligned}\min C_{\mathrm{VPPO}} &= f_{\mathrm{gas}}\sum_{t=1}^{T}\left(P_{t,\mathrm{gas}}^{\mathrm{CHP}}+P_{t,\mathrm{gas}}^{\mathrm{GB}}\right)+f_{\mathrm{ESS}}\sum_{t=1}^{T}P_{t}^{\mathrm{dis}}\\&+\mathrm{c}\,f_{\mathrm{dis}}\sum_{t=1}^{T}\left(P_{t,\mathrm{pv}}^{\mathrm{VPPO}}-P_{t,\mathrm{pv}}^{\mathrm{VPPO,real}}\right)+f_{\mathrm{dis}}\sum_{t=1}^{T}\left(P_{t,\mathrm{wt}}^{\mathrm{VPPO}}-P_{t,\mathrm{wt}}^{\mathrm{VPPO,real}}\right)\\&+\sum_{t=1}^{T}\left(p_{t,\mathrm{e}}^{\mathrm{buy}}P_{t,\mathrm{e}}^{\mathrm{buy}}-p_{t,\mathrm{e}}^{\mathrm{sell}}P_{t,\mathrm{e}}^{\mathrm{sell}}\right)-\sum_{t=1}^{T}\left(p_{t,\mathrm{h}}^{\mathrm{opt}}P_{t,\mathrm{e}}^{\mathrm{real,load}}+p_{t,\mathrm{h}}^{\mathrm{opt}}P_{t,\mathrm{h}}^{\mathrm{real,load}}\right)\end{aligned} \tag{1}$$

where f_{gas} denotes the unit price of natural gas; $P_{t,\mathrm{gas}}^{\mathrm{CHP}}P_{t,\mathrm{gas}}^{\mathrm{GB}}$ represent the gas consumption of Combined thermal and Power (CHP)/ Gas boiler (GB) at time t; f_{ESS} represents the unit power generation cost of energy storage;P_{t}^{dis} represent the discharging power of the electrical energy storage respectively; f_{dis} represents the unit for non consumption of new energy; $P_{t,\mathrm{wt}}^{\mathrm{VPPO,real}}P_{t,\mathrm{pv}}^{\mathrm{VPPO,real}}$ represent the actual output of the wind turbine (WT) and the PV at time t; $P_{t,\mathrm{wt}}^{\mathrm{VPPO}}P_{t,\mathrm{pv}}^{\mathrm{VPPO}}$ represent the predicted power generation capacity of WT and PV generators at time t. $p_{t,\mathrm{e}}^{\mathrm{buy}}P_{t,\mathrm{e}}^{\mathrm{buy}}P_{t,\mathrm{h}}^{\mathrm{buy}}$ represent the purchase and sale electricity price/thermal price with the external power grid/thermal network at time t; $p_{t,\mathrm{e}}^{\mathrm{opt}}p_{t,\mathrm{h}}^{\mathrm{opt}}$ represent the optimized electricity price and thermal price passed to the followers by VPPO at time t; $P_{t,\mathrm{e}}^{\mathrm{real,load}}P_{t,\mathrm{h}}^{\mathrm{real,load}}$ represent the optimized load;

CHP is a device that generates both electricity and thermal simultaneously. The model is:

$$\begin{cases} P_{t,\mathrm{e}}^{\mathrm{CHP}} = \eta_{e}^{\mathrm{CHP}} P_{t,\mathrm{gcx}}^{\mathrm{CHP}} q_{\mathrm{gas}} \\ P_{t,\mathrm{h}}^{\mathrm{CHP}} = \eta_{\mathrm{h}}^{\mathrm{CHP}} P_{t,\mathrm{gcx}}^{\mathrm{CHP}} q_{\mathrm{gas}} \\ P_{\mathrm{min,e}}^{\mathrm{CHP}} \le P_{t,\mathrm{e}}^{\mathrm{CHP}} \le P_{\mathrm{max,e}}^{\mathrm{CHP}} \\ P_{\mathrm{min,h}}^{\mathrm{CHP}} \le P_{t,\mathrm{h}}^{\mathrm{CHP}} \le P_{\mathrm{max,h}}^{\mathrm{CHP}} \end{cases} \tag{2}$$

where $P_{t,\mathrm{e}}^{\mathrm{CHP}} P_{t,\mathrm{h}}^{\mathrm{CHP}}$ represent the power generation and thermal generation of CHP at time t; $\eta_{\mathrm{e}}^{\mathrm{CHP}}$ represents the thermal generation efficiency of CHP; q_{gas} represents the calorific value of natural gas combustion; $P_{\mathrm{min,e}}^{\mathrm{CHP}} P_{\mathrm{max,e}}^{\mathrm{CHP}}$ represent the minimum/maximum generating power of CHP; $P_{\mathrm{min,h}}^{\mathrm{CHP}} P_{\mathrm{max,h}}^{\mathrm{CHP}}$ represent the minimum/maximum thermal generation power of CHP respectively.

GB as the main thermal energy supply equipment in the VPP, generates thermal energy by burning natural gas. The model is as follows:

$$\begin{cases} P_{t,\mathrm{h}}^{\mathrm{GB}} = P_{t,\mathrm{gas}}^{\mathrm{GB}} \theta_{h}^{\mathrm{GB}} Q_{\mathrm{gas}} \\ P_{\mathrm{min,h}}^{\mathrm{GB}} \le P_{t,\mathrm{h}}^{\mathrm{GB}} \le P_{\mathrm{max,h}}^{\mathrm{GB}} \end{cases} \tag{3}$$

where $P_{t,\mathrm{h}}^{\mathrm{GB}}$ represents the thermal dissipation power of GB at time t; $\theta_{\mathrm{h}}^{\mathrm{GB}}$ represents the thermal production efficiency of the GB; $P_{\mathrm{min,h}}^{\mathrm{GB}} P_{\mathrm{max,h}}^{\mathrm{GB}}$ represent the minimum/maximum thermal generation power of GB at time t.

VPPO store and retrieve electricity through electric energy storage devices to balance internal power generation and the purchase and sale of electricity from the external power grid. The model is as follows:

$$\begin{cases} E_{t+1}^{\mathrm{ESS}} = (1-\omega_{e}) E_{t}^{\mathrm{ESS}} + \omega_{\mathrm{chr}} P_{t+1}^{\mathrm{chr}} - P_{t+1}^{\mathrm{dis}} / \omega_{\mathrm{dis}} \\ E_{\mathrm{min}}^{\mathrm{ESS}} \le E_{t}^{\mathrm{ESS}} \le E_{\mathrm{max}}^{\mathrm{ESS}} \\ U_{t.\mathrm{chr}} P_{\mathrm{chr}}^{\mathrm{min}} \le P_{t}^{\mathrm{chr}} \le U_{t.\mathrm{chr}} P_{\mathrm{chr}}^{\mathrm{max}} \\ U_{t.\mathrm{dis}} P_{\mathrm{dis}}^{\mathrm{min}} \le P_{t}^{\mathrm{dis}} \le U_{t.\mathrm{dis}} P_{\mathrm{dis}}^{\mathrm{max}} \\ U_{t.\mathrm{chr}} + U_{t.\mathrm{dis}} \le 1 \\ P_{\mathrm{cl,chr}}^{\mathrm{min}} \le P_{t+1}^{chr} - P_{t}^{chr} \le P_{\mathrm{cl,chr}}^{\mathrm{max}} \\ P_{\mathrm{cl,dis}}^{\mathrm{min}} \le P_{t+1}^{\mathrm{dis}} - P_{t}^{\mathrm{dis}} \le P_{\mathrm{cl,dis}}^{\mathrm{max}} \end{cases} \tag{4}$$

where E_{t}^{ESS} represents the state of charge of the electrical energy storage; $\omega_{\mathrm{chr}} \omega_{\mathrm{dis}}$ represent the charging/discharging efficiency of electrical energy storage; $U_{t.\mathrm{chr}} U_{t.\mathrm{dis}}$ represent the state marking bit; $P_{\mathrm{cl,chr}}^{\mathrm{min}} P_{\mathrm{cl,dis}}^{\mathrm{min}} P_{\mathrm{cl,dis}}^{\mathrm{max}} P_{\mathrm{cl,chr}}^{\mathrm{max}} P_{\mathrm{cl,dis}}^{\mathrm{max}}$ represent the minimum/maximum charging/discharging powers of the electric energy storage in the charging/discharging state.

VPPO integrate wind and photovoltaic resources for power supply. The actual power generation is within the predicted power generation date. Therefore, the models for WT and PV are:

$$\begin{cases} 0 \le P_{t,\mathrm{wt}}^{\mathrm{VPPO,real}} \le P_{t,\mathrm{wt}}^{\mathrm{VPPO}} \\ 0 \le P_{t,\mathrm{pv}}^{\mathrm{VPPO,real}} \le P_{t,\mathrm{pv}}^{\mathrm{VPPO}} \end{cases} \tag{5}$$

When the internal CHP and GB of VPPO fail to meet the demands of PVP, they need to purchase additional electricity and thermal from the external power grid and external thermal network. Meanwhile, when there is an excess of energy, they can also sell the energy to obtain additional benefits. The model is as follows:

$$\begin{cases} 0 \le P_{t,\mathrm{e}}^{\mathrm{buy}} \le U_{t.\mathrm{e}}^{\mathrm{buy}} P_{\mathrm{e,buy}}^{\mathrm{max}} \\ 0 \le P_{t,\mathrm{e}}^{\mathrm{sell}} \le U_{t.\mathrm{e}}^{\mathrm{sell}} P_{\mathrm{e,sell}}^{\mathrm{max}}, \\ U_{t.\mathrm{e}}^{\mathrm{buy}} + U_{t.\mathrm{e}}^{\mathrm{sell}} \le 1 \end{cases} \quad \begin{cases} 0 \le P_{t,\mathrm{h}}^{\mathrm{buy}} \le U_{t.\mathrm{h}}^{\mathrm{buy}} P_{\mathrm{h,buy}}^{\mathrm{max}} \\ 0 \le P_{t,\mathrm{h}}^{\mathrm{sell}} \le U_{t.\mathrm{h}}^{\mathrm{sell}} P_{\mathrm{h,sell}}^{\mathrm{max}} \\ U_{t.\mathrm{h}}^{\mathrm{buy}} + U_{t.\mathrm{h}}^{\mathrm{sell}} \le 1 \end{cases} \tag{6}$$

where $P_{t,\mathrm{e}}^{\mathrm{buy}} P_{t,\mathrm{h}}^{\mathrm{buy}} P_{t,\mathrm{e}}^{\mathrm{sell}} P_{t,\mathrm{h}}^{\mathrm{sell}}$ represent the electricity/thermal loads purchased/sold by VPPO to the external power grid and the external thermal network at time t; $P_{\mathrm{e,buy}}^{\mathrm{min}} P_{\mathrm{h,buy}}^{\mathrm{min}} P_{\mathrm{e,sell}}^{\mathrm{min}} P_{\mathrm{h,sell}}^{\mathrm{min}}$ represent the maximum electric and thermal load purchased/sold by the VPPO operation from the external power grid thermal network; The flag bits representing the trading situation at time t respectively.

Comprehensively considering the output strategy of the VPP operator, the thermal power balance of the VPPO i at time t can be obtained as:

$$\begin{aligned} &P_{t,\mathrm{e}}^{\mathrm{buy}} - P_{t,\mathrm{e}}^{\mathrm{sel}} + P_{t,\mathrm{e}}^{\mathrm{CHP}} + P_{t,\mathrm{wt}}^{\mathrm{VPPO,real}} + P_{t,\mathrm{pv}}^{\mathrm{VPPO,real}} + \\ &P_{t}^{\mathrm{dis}} - P_{t}^{\mathrm{chr}} - P_{i,j,e,t}^{\mathrm{P2P}} - P_{j,i,e,t}^{\mathrm{P2P}} = P_{t,\mathrm{e}}^{\mathrm{load,reai}}, \forall i \neq j \\ &P_{t,\mathrm{h}}^{\mathrm{buy}} - P_{t,\mathrm{h}}^{\mathrm{sel}} + P_{t,\mathrm{h}}^{\mathrm{CHP}} + P_{t,\mathrm{h}}^{\mathrm{GB}} + \\ &P_{t,\mathrm{h}}^{\mathrm{cut}} - P_{i,j,h,t}^{\mathrm{P2P}} - P_{j,i,h,t}^{\mathrm{P2P}} = P_{t,h}^{\mathrm{load,reai}}, \forall i \neq j \end{aligned} \tag{7}$$

where $P_{t,\mathrm{e}}^{\mathrm{load,reai}} P_{t,\mathrm{h}}^{\mathrm{load,reai}}$ represent the optimized load demand of the follower photovoltaic consumer after the demand response, that is, the actual thermal and electricity load purchased from the leader, which is included as the revenue portion in the objective function. $P_{i,j,e,t}^{P2P} P_{j,i,h,t}^{\mathrm{P2P}}$ respectively represents the electricity and thermal sold by the VPP i to the VPP j at time t;

1.3 PVP model

PVP are users who possess both the capacity for photovoltaic power generation and the demand for electricity and heat energy. The cost of PVP consists of three parts: the cost of purchasing electricity and thermal from leading VPPO, the cost obtained from demand response, and the cost generated from wind and solar power curtailment. The objective function of PVP is:

$$\begin{aligned} &\min C_{\mathrm{PVP}}^{\mathrm{non}} = \sum_{t=1}^{T} \left(p_{t,\mathrm{e}}^{\mathrm{opt}} P_{t,\mathrm{e}}^{\mathrm{real,load}} + p_{t,\mathrm{h}}^{\mathrm{opt}} P_{t,\mathrm{h}}^{\mathrm{real,load}} \right) + \\ &\sum_{t=1}^{T} \left(P_{t,\mathrm{e}}^{\mathrm{cut}} f_{t,\mathrm{e}}^{\mathrm{cut}} + P_{t,\mathrm{h}}^{\mathrm{cut}} f_{t,\mathrm{h}}^{\mathrm{cut}} \right) + f_{\mathrm{pv}}^{\mathrm{dis}} \sum_{t=1}^{T} \left(P_{t,\mathrm{pv}}^{\mathrm{DPP}} - P_{t,\mathrm{pv}}^{\mathrm{DPP,real}} \right) \end{aligned} \tag{8}$$

where the cost of electricity/thermal load can be reduced in units of $f_{t,\mathrm{e}}^{\mathrm{cut}} f_{t,\mathrm{h}}^{\mathrm{cut}}$; $P_{t,\mathrm{e}}^{\mathrm{cut}} P_{t,\mathrm{h}}^{\mathrm{cut}}$ represent the reduction in electricity/thermal load at time t; $P_{t,\mathrm{pv}}^{\mathrm{DPP,real}}$ represents the actual output of the photovoltaic power generation at time t; $P_{t,\mathrm{pv}}^{\mathrm{PVP}}$ represents the predicted power generation capacity of the photovoltaic power generation unit at time t;

The load reducible model in demand response is:

$$\begin{cases} P^{\text{cut}}_{\text{min,e}} \le P^{\text{cut}}_{t,\text{e}} \le P^{\text{cut}}_{\text{max,e}}, \forall t \in \mu^1_t, \mu^2_t \\ P^{\text{cut}}_{\text{min,h}} \le P^{\text{cut}}_{t,\text{h}} \le P^{\text{cut}}_{\text{max,h}}, \forall t \in \mu^3_t, \mu^4_t \end{cases} \tag{9}$$

where $P^{\text{cut}}_{\text{min,e}} P^{\text{cut}}_{\text{max,e}}$ and $P^{\text{cut}}_{\text{min,h}} P^{\text{cut}}_{\text{max,h}}$ represent the minimum/-maximum reduction amounts of electricity/thermal load; $\mu^1_t\ \mu^2_t\ \mu^3_t\ \mu^4_t$ are the Lagrange multiplier of the inequality constraint Eq. (9).

PVP only integrate photovoltaic resources for internal power supply. The model is:

$$0 \le P^{\text{PVP,real}}_{t,\text{pv}} \le P^{\text{PVP}}_{t,\text{pv}}, \forall t \in \mu^5_t, \mu^6_t \tag{10}$$

where $\mu^5_t\ \mu^6_t$ are the Lagrange multiplier of the inequality constraint Eq. (10).

Comprehensively considering the demand response of PVP, the thermal power balance at time t can be obtained as:

$$\begin{aligned} P^{\text{load,real}}_{t,\text{e}} &= P^{\text{Load}}_{t,\text{e}} - P^{\text{PVP,real}}_{t,\text{pv}} + P^{\text{sl,in}}_{t,\text{e}} \\ &\quad - P^{\text{sl,out}}_{t,\text{e}} - P^{\text{cut}}_{t,\text{e}}, \forall t \in \lambda^1_t \\ P^{\text{load,real}}_{t,\text{h}} &= P^{\text{Load}}_{t,\text{h}} - P^{\text{cut}}_{t,\text{h}}, \forall t \in \lambda^2_t \end{aligned} \tag{11}$$

where $\lambda^1_t \lambda^2_t$ are the Lagrange multipliers of the equation constraint Eq. (11).

2 Multiple uncertainty modeling of VPPs

2.1 Improved fuzzy opportunistic constraint model based on generalized credibility

The fuzzy chance constraint method is used to model source-load uncertainty in this paper. This method allows the optimal solution to violate constraint criteria to a certain extent, but the chance of satisfying all constraints must not be lower than the pre-set confidence level [21,22]. The fuzzy chance constraint of a fuzzy constraint is:

$$\begin{cases} \min f(x, \omega) \\ \text{s.t.} Cr\left\{ \omega : \mu_{g\left(x,\widetilde{\theta}\right)(\omega) \le 0} \right\} \ge \alpha \end{cases} \tag{12}$$

where w is an element in the sample space, $\mu_{g\left(x,\widetilde{\theta}\right)(\omega) \le 0}$ is the membership function of the fuzzy event $g\left(x, \widetilde{\theta}\right) \le 0$, and $\alpha \in [0,1]$ is a given confidence level.

Power fluctuations on generation and demand sides exhibit distinct risk characteristics across different temporal periods. During high-risk intervals—characterized by peak electricity and thermal consumption coinciding with volatile renewable generation and prosumer load—the VPPO prioritizes power supply and heating reliability assurance. Conversely, during low-risk periods where renewable output is sufficient and load demand is subdued. This enables the VPPO to strategically modulate control stringency over uncertainties due to increased system flexibility. Conversely, during low-risk periods, VPPO can appropriately relax the control requirements for uncertain factors because it has a higher operating margin.

According to the above analysis, the trapezoidal fuzzy set $\widetilde{P}_t$ of the source load power in period t is:

$$\widetilde{P}_t = (P_t\eta_1, P_t\eta_2, P_t\eta_3, P_t\eta_4) \tag{13}$$

where η_1 and η_4 represent the left and right endpoints of the trapezoidal fuzzy set; η_2 and η_3 represent the lower and upper bounds of the core interval of the trapezoidal fuzzy set, and the membership function $\widetilde{P}_t$ of its trapezoidal fuzzy set is:

$$\mu_r\left(\widetilde{P}_t\right) = \begin{cases} 0\ ,\ \widetilde{P}_t \le P_t\eta_1 \text{ or } \widetilde{P}_t \ge P_t\eta_4 \\ \frac{\widetilde{P}_t - P_t\eta_1}{P_t\eta_2 - P_t\eta_1},\ P_t\eta_1 \le \widetilde{P}_t \le P_t\eta_2 \\ 1\ ,\ P_t\eta_2 \le \widetilde{P}_t \le P_t\eta_3 \\ \frac{P_t\eta_4 - \widetilde{P}_t}{P_t\eta_4 - P_t\eta_3},\ P_t\eta_3 \le \widetilde{P}_t \le P_t\eta_4 \end{cases} \tag{14}$$

where $\widetilde{P}_t$ takes different values in different fuzzy sets. When the membership degree value is 1, $\widetilde{P}_t$ is in the fuzzy core interval, which is at the top of the trapezoid. When the membership degree value is between (0,1), it is on the two hypotenuses of the trapezoid. When the membership degree function is 0, it indicates that $\widetilde{P}_t$ does not belong to any fuzzy interval.

Based on the literatures [21,22], this paper improves the clear equivalence class method of the traditional trapezoidal fuzzy set. According to the traditional credibility measure, it is finally derived that the weights corresponding to the right endpoint η_3 of the upper bottom and the right endpoint η_4 of the lower bottom of the trapezoidal are (2-2α) and (2α-1). In this model, the confidence information in the two directions of possibility and necessity is the same. That is:

$$Cr\left\{ g\left(x, \widetilde{P}\right) \right\} = \frac{1}{2} Poss\{g\} + \frac{1}{2} Nec\{g\} \tag{15}$$

where *Poss* (Possibility Measure) represents the possibility measure, that is, whether an event is likely to occur; *Nec* (Necessity Measure) represents the measure of necessity, that is, whether an event is bound to occur. Two measures are used to describe the occurrence probability of fuzzy events.

In this paper, the traditional clear equivalence class Eq. (15) is improved by using the generalized credibility theory. Different types of risk preferences are set for the source charge data in different risk periods for classification and discussion. The risk preference coefficient β_c is introduced and defined as:

$$Cr\left\{ g\left(x, \widetilde{P}\right) \right\} = \beta_t Poss\{g\} + (1 - \beta_t) Nec\{g\} \tag{16}$$

where β_t enables the VPP to be regulated between *Poss* and *Nec*, and $\beta_t \in [0,1]$. When *Nec* is 1, it indicates that all situations must support the validity of the fuzzy event. When

Poss is 1, it indicates that there exists a certain situation that supports the validity of the fuzzy event.

Therefore, by controlling the value of β_t, it is possible to reflect the different risk preferences of the VPP for various uncertain events. When $\beta_t > 0.5$, $Nec > Poss$, and more attention is paid to the situation where the fuzzy events are almost certain not to occur, which belongs to a conservative risk preference strategy. Conversely, when $\beta_t < 0.5$, $Nec < Poss$, and more attention is paid to the maximum extent to which the event is likely to occur, which belongs to an optimistic risk preference strategy.

Taking the right descending segment of the trapezoidal fuzzy set as an example, the derivation process of the clear equivalence class after introducing β_t is shown in Appendix A. Finally, the weight Settings of the clear equivalence class of the trapezoidal fuzzy set under generalized credibility and the corresponding risk preference types are presented in Table 2.

In conclusion, after considering the source loads with different risk preferences and adopting the clear equivalence class formula, the equivalent power load balance for the VPPO in Eq. (7) is:

$$\begin{aligned}&\tfrac{1-\alpha}{\beta_t}\left(P_{t,\mathrm{e}}^{\mathrm{load,reai}}\eta_3 - P_{t,\mathrm{wt}}^{\mathrm{VPPO,real}}\eta_2 - P_{t,\mathrm{pv}}^{\mathrm{VPPO,real}}\eta_2\right)+\\&\tfrac{\alpha-(1-\beta_t)}{\beta_t}\left(P_{t,\mathrm{e}}^{\mathrm{load,reai}}\eta_4 - \widetilde{P}_{c,\mathrm{wt}}^{\mathrm{VPPO,real}}P_{t,\mathrm{wt}}^{\mathrm{VPPO,real}}\eta_1 - P_{t,\mathrm{pv}}^{\mathrm{VPPO,real}}\eta_1\right)-\\&P_{t,\mathrm{e}}^{\mathrm{buy}} + P_{t,\mathrm{e}}^{\mathrm{sell}} - P_{t,\mathrm{e}}^{\mathrm{CHP}} - P_{t}^{\mathrm{dis}} + P_{t}^{\mathrm{chr}} + P_{i,j,e,t}^{\mathrm{P2P}} + P_{j,i,e,t}^{\mathrm{P2P}} = 0\end{aligned} \tag{17}$$

For the thermal load balance equivalence of the VPPO in Eq. (7), it is:

$$\begin{aligned}&\tfrac{1-\alpha}{\beta_t}P_{t,\mathrm{h}}^{\mathrm{load,reai}}\eta_3 + \tfrac{\alpha-(1-\beta_t)}{\beta_t}P_{t,\mathrm{h}}^{\mathrm{load,reai}}\eta_4-\\&P_{t,\mathrm{h}}^{\mathrm{buy}} + P_{t,\mathrm{h}}^{\mathrm{sell}} - P_{t,\mathrm{h}}^{\mathrm{CHP}} - P_{t,\mathrm{h}}^{\mathrm{GB}} - P_{t,\mathrm{h}}^{\mathrm{cut}} + P_{i,j,h,t}^{\mathrm{P2P}} + P_{j,i,h,t}^{\mathrm{P2P}} = 0\end{aligned} \tag{18}$$

For the electricity load balance equivalence of PVP in Eq. (11), it is:

$$\begin{aligned}&\tfrac{1-\alpha}{\beta_t}P_{t,e}^{\mathrm{load,reai}}\eta_3 + \tfrac{\alpha-(1-\beta_t)}{\beta_t}P_{t,e}^{\mathrm{load,reai}}\eta_4 - P_{t,e}^{\mathrm{Load}}\\&+(2-2\alpha)P_{t,pv}^{\mathrm{DPP,real}}\eta_2 + (2\alpha-1)\eta_1 P_{t,pv}^{\mathrm{DPP,real}} + P_{t,e}^{\mathrm{cut}} = 0\end{aligned} \tag{19}$$

For the thermal load balance equivalence of PVP in Eq. (11), it is:

$$\begin{aligned}&\tfrac{1-\alpha}{\beta_t}P_{t,\mathrm{h}}^{\mathrm{load,reai}}\eta_{\mathrm{c},3} + \tfrac{\alpha-(1-\beta_t)}{\beta_t}P_{t,\mathrm{h}}^{\mathrm{load,reai}}\eta_4\\&-P_{t,\mathrm{h}}^{\mathrm{Load}} + P_{t,\mathrm{h}}^{\mathrm{cut}} = 0\end{aligned} \tag{20}$$

Meanwhile, this paper takes into account the uncertainty of $P_{t,\mathrm{pv}}^{\mathrm{PVP,real}}$ and adopts the traditional trapezoidal fuzzy chance-constrained method. The clear equivalent process is presented in Appendix A. The modification process of the KKT equilibrium condition is presented in Appendix C. After the above Eq. (18)-(21) are processed by clear equivalence classes, the commercial optimization software CPLEX can be directly used to solve the model.

Table 2
Weight setting and risk preference types under generalized credibility.

β_t	Risk preference type	Left weight	Right weight
$\beta_t > 0.5$	Conservative type	$\frac{1-\alpha}{\beta_t}$	$\frac{\alpha-(1-\beta_t)}{\beta_t}$
$\beta_t = 0.5$	Neutral	$2-2\alpha$	$2\alpha-1$
$\beta_t < 0.5$	Optimistic type	$\frac{1-\alpha}{\beta_t}$	$\frac{\alpha-(1-\beta_t)}{\beta_t}$

2.2 Robust optimization model considering price fluctuations

During the operation of VPPs, the frequent fluctuations in electricity and thermal prices will not only increase their own operating costs, but also further affect the Nash bargaining process among multiple VPPs. By adopting the robust optimization method, the cost risk caused by price fluctuations can be effectively reduced by solving the optimal operation strategy in the worst scene [23].

In the period set within the dispatching cycle T, the fluctuation coefficient $\varphi_{\mathrm{e}}\varphi_{\mathrm{h}}$ of electricity and thermal prices in different periods is considered to measure the degree of price fluctuation in that period. At the same time, set Γ as the number of periods with uncertainties in electricity prices and thermal prices, $0 \le \Gamma \le T$. Define the binary variables $U_{t,\mathrm{e}}^{\varphi}$ and $U_{t,\mathrm{h}}^{\varphi}$. When $U_{t,\mathrm{e}}^{\varphi}$ and $U_{t,\mathrm{h}}^{\varphi}$ are 1, it represents the period t considering the influence of the electricity price fluctuation coefficient $\varphi_e\,\varphi_h$, that is, the period in which the fluctuations of electricity prices and thermal prices are severe. When $U_{t,\mathrm{e}}^{\varphi}$ and $U_{t,\mathrm{h}}^{\varphi}$ are 0, it indicates that the uncertainties of electricity and thermal prices are not taken into account. To sum up, in the objective function, the fluctuation penalty cost term considering electricity prices and thermal prices is expressed as.

$$\begin{cases}\max \sum_{c=1}^{C}\sum_{t\in c}^{T_C}\left[\varphi_{\mathrm{e}}P_{t,\mathrm{e}}^{\mathrm{load,reai}}U_{t,\mathrm{e}}^{\varphi} + \varphi_{\mathrm{h}}P_{\mathrm{h,e}}^{\mathrm{load,reai}}U_{t,\mathrm{e}}^{\varphi}\right]\\ \text{s.t.}\begin{cases}\sum_{t=1}^{T}U_{t,\mathrm{e}}^{\varphi} \le \Gamma, \sum_{t=1}^{T}U_{t,\mathrm{h}}^{\varphi} \le \Gamma\\ 0 \le U_{t,\mathrm{e}}^{\varphi} \le 1, 0 \le U_{t,\mathrm{h}}^{\varphi} \le 1\end{cases}\end{cases} \tag{21}$$

Combining Eq. (1), the running objective function of VPP is as follows:

$$\begin{aligned}&\min C_{\mathrm{VPPO}}^{\mathrm{non}} = C_{\mathrm{VPPO}}+\\&\max \sum_{t=1}^{T}\left[\varphi_{\mathrm{e}}P_{t,\mathrm{e}}^{\mathrm{load,reai}}U_{t,\mathrm{e}}^{\varphi} + \varphi_{\mathrm{h}}P_{\mathrm{h,e}}^{\mathrm{load,reai}}U_{t,\mathrm{e}}^{\varphi}\right]\end{aligned} \tag{22}$$

where the max term is the price fluctuation penalty term caused by the uncertainty of electricity and thermal prices, which is introduced into the objective function. The purpose is to mitigate the impact caused by the fluctuations of electricity and thermal prices. Therefore, the optimal operating cost needs to be considered under the maximum risk. The objective function belongs to the min–max robust optimization problem. For this problem, the dual variables are set as follows:

$$\begin{cases} \Gamma - \sum_{t=1}^{T} U_{t,\mathrm{e}}^{\varphi} \geq 0 \rightarrow \varsigma_1 \\ \Gamma - \sum_{t=1}^{T} U_{t,\mathrm{h}}^{\varphi} \geq 0 \rightarrow \varsigma_2 \\ 1 - U_{t,\mathrm{e}}^{\varphi} \geq 0 \rightarrow \varsigma_3 \\ 1 - U_{t,\mathrm{h}}^{\varphi} \geq 0 \rightarrow \varsigma_4 \\ U_{t,\mathrm{e}}^{\varphi} \geq 0 \rightarrow \varsigma_5 \\ U_{t,\mathrm{h}}^{\varphi} \geq 0 \rightarrow \varsigma_6 \end{cases} \tag{23}$$

The derivation process is shown in Appendix B. Through the transformation in Appendix B, the min–max problem is equivalent to:

$$\mathrm{c}\begin{cases} \min \sum_{t=1}^{T} (\varsigma_1 \Gamma + \varsigma_2 \Gamma + \varsigma_3 + \varsigma_4) \\ \text{s.t.} \begin{cases} \varsigma_1 + \varsigma_3 \geq \varphi_e \widehat{P}_{e,0}, \varsigma_2 + \varsigma_4 \geq \varphi_h \widehat{P}_{h,0} \\ -\widehat{P}_{e,0} \leq P_{t,e}^{\mathrm{load,reai}} \leq \widehat{P}_{e,0} \\ -\widehat{P}_{h,0} \leq P_{t,h}^{\mathrm{load,reai}} \leq \widehat{P}_{h,0} \\ \widehat{P}_{e,0} \geq 0, \widehat{P}_{h,0} \geq 0 \\ \varsigma_1 \geq 0, \varsigma_2 \geq 0, \varsigma_3 \geq 0, \varsigma_4 \geq 0 \end{cases} \end{cases} \tag{24}$$

Therefore, through dual equivalent transformation, the final Eq. (22) is transformed into:

$$\min C_{\mathrm{VPPO}}^{\mathrm{non}} = \min \left\{ C_{\mathrm{VPPO}} + \left(\sum_{t=1}^{T} \varsigma_1 \Gamma + \varsigma_2 \Gamma + \varsigma_3 + \varsigma_4 \right) \right\} \tag{25}$$

2.3 Framework for modeling multiple uncertainties

From the perspective of uncertainty modeling. The uncertain variables involved in this paper include: the output of new energy, load demand, and market prices. Among them, the output of new energy and load demand can be obtained through statistical methods based on historical data, and their probability distributions can be calculated. Therefore, the fuzzy chance-constrained method was adopted to deal with the perturbation caused by the deviation of the prediction of new energy output and user load demand. Considering that the uncertainty of market prices is affected by external factors such as policy regulation, it is difficult to obtain an accurate probability distribution. Therefore, this paper adopts the robust optimization method to deal with the uncertainty of electricity prices. Together, these two methods address multiple uncertainties faced during the operation of VPP. The uncertainty modeling framework of this paper is shown in Fig. 2.

From the perspective of the VPP operation optimization model constructed in this paper, the uncertainty of the sources and loads mainly manifests in the constraints, while the uncertainty of the market price is mainly reflected in the objective function. Therefore, the fuzzy chance-constrained and robust optimization methods respectively model the uncertainty for different types of variables, and the two work together to achieve the overall optimization result of the VPP operation optimization model.

3 VPP Nash-Stackelberg game model

3.1 Stackelberg game model

For the Stackelberg game model composed of VPPO and PVP, this paper equivalently transforms the follower prosumer model by constructing the Lagrange function and using the KKT condition. Apply the strong duality method, which was adopted to relax the energy purchase costs $p_{t,\mathrm{e}}^{\mathrm{opt}} P_{t,\mathrm{e}}^{\mathrm{real,load}}$ and $p_{t,\mathrm{h}}^{\mathrm{opt}} P_{t,\mathrm{h}}^{\mathrm{real,load}}$ of prosumers. The specific derivation process is shown in Appendix C. Finally, it was transformed into a single-layer linear programming model as follows:

$$\begin{cases} \min C_{\mathrm{VPPO}}^{\mathrm{non}} \\ \text{s.t.} \begin{cases} (2)-(6), (9)-(10), (17)-(20), \\ (B3), (C2), (C4), (C7) \end{cases} \end{cases} \tag{26}$$

g

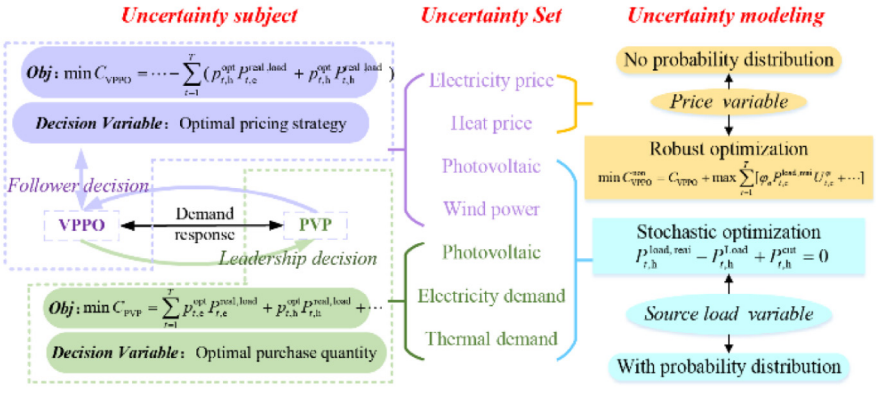

Fig. 2. Framework for Modeling Multiple Uncertainties.

3.2 Multi VPP cooperative game model

Under the Nash-Stackelberg game framework, the Nash bargaining model, as a cooperative game mechanism, maximizes the overall interests of the VPP alliance while completing the distribution of cooperative benefits through bargaining. This paper considers the standard Nash bargaining model, ensuring that the bargaining positions of the n VPPs participating in the Nash bargaining are the same, that is, λ_i is all 1. Since the cost and benefit are opposite to each other, thus there is:

$$\begin{cases} \max \prod_{i=1}^{n} \left(C_{\mathrm{VPPi}}^{\mathrm{non}} - C_{\mathrm{VPPi}}^{\mathrm{coo}}\right)^{\lambda_i} \\ \text{s.t.} \begin{cases} C_{\mathrm{VPP}i}^{\mathrm{non}} \geq C_{\mathrm{VPP}i}^{\mathrm{coo}} \\ (2)-(6),(9)-(10),(17)-(20), \\ (B3),(C2),(C4),(C7) \end{cases} \end{cases} \tag{27}$$

where n represents the number of entities participating in the Nash-Stackelberg game; $C_{\mathrm{VPP}i}^{\mathrm{coo}}$ represents the total cost of the VPP i after the Nash bargaining; $C_{\mathrm{VPP}i}^{\mathrm{non}}$ represents the total cost of the VPP i when the bargaining breaks down, that is, the total cost when considering the Stackelberg game model.

The above equation is a non-convex nonlinear problem. To further simplify the model solution, the mean value inequality method [24] is adopted to simplify it into two linearly separable subproblems. The specific model is as follows:

SP1: Minimizing the operating cost of the VPP Alliance in a multi-uncertainty environment:

$$\begin{cases} \min \sum_{i=1}^{n} C_{\mathrm{VPP}i}^{\mathrm{coo}} \\ \text{s.t.} \begin{cases} (2)-(6),(9)-(10),(17)-(20), \\ (B3),(C2),(C4),(C7) \end{cases} \end{cases} \tag{28}$$

where the P2P transaction costs of electrical energy and thermal energy are ignored in SP1, with $\sum_i \sum_j P_{i,j,e,t}^{\mathrm{P2P}} = 0$, so there is multiple coupling among the three VPPs. Therefore, the auxiliary variables $P_{i,j,e,t}^{\mathrm{P2P}}$ and $P_{i,j,h,t}^{\mathrm{P2P}}$ are introduced to transform SP1 into a dual-coupled model as follows:

$$\begin{cases} P_{i,j,e,t}^{\mathrm{P2P}} = -P_{j,i,e,t}^{\mathrm{P2P}}, \forall i \neq j \\ P_{i,j,h,t}^{\mathrm{P2P}} = -P_{j,i,h,t}^{\mathrm{P2P}}, \forall i \neq j \end{cases} \tag{29}$$

where $P_{i,j,e,t}^{\mathrm{P2P}} P_{i,j,h,t}^{\mathrm{P2P}}$ are the introduced auxiliary variables. It indicates that a consensus on the trading of electrical and thermal energy has been reached between VPP i and j. After decoupling, subsequent distributed solutions can be carried out.

SP2: VPP Alliance maximizes revenue distribution

$$\begin{cases} \min \sum_{i=1}^{n} -\ln\left[C_{\mathrm{VPP}i}^{\mathrm{non}} - \left(C_{\mathrm{VPP}i}^{\mathrm{coo}} + C_{\mathrm{VPP}i}^{\mathrm{p2p}}\right)\right] \\ \text{s.t.} \left\{C_{\mathrm{VPP}i}^{\mathrm{non}} \geq \left(C_{\mathrm{VPP}i}^{\mathrm{coo}} + C_{\mathrm{VPP}i}^{\mathrm{p2p}}\right)\right. \end{cases} \tag{30}$$

The decoupling is the same as the processing method of SP1, with the following double coupling constraints:

$$\begin{cases} p_{i,j,e,t}^{\mathrm{P2P}} = p_{j,i,e,t}^{\mathrm{P2P}}, \forall i \neq j \\ p_{i,j,h,t}^{\mathrm{P2P}} = p_{j,i,h,t}^{\mathrm{P2P}}, \forall i \neq j \end{cases} \tag{31}$$

where $p_{i,j,e,t}^{\mathrm{P2P}} p_{i,j,h,t}^{\mathrm{P2P}}$ represent the expected transaction electricity price and thermal price solved in SP1. When the equation relationship is satisfied, it indicates that VPP i and j have reached a consensus on the transaction of electricity price and thermal price, and can be solved in a distributed manner in the future with SP1.

3.3 Model solving process

First, solve the Stackelberg game model to obtain the breakdown point of the Nash bargaining. Next, distributed solutions need to be carried out for SP1 and SP2. ADMM is adopted for distributed solution, and the subproblems corresponding to each VPP are decomposed by setting the coupling constraints Eqs. (29) and (31). For the VPP i, the augmented Lagrangian function of SP1 is obtained as follows:

$$L_i^{\mathrm{SP2}}\left(p_{i,j,e,t}, p_{i,j,h,t}\right) = \min\Bigg\{-\ln\left[\left(C_{\mathrm{VPP}i}^{\mathrm{non}} - C_{\mathrm{VPP}i}^{\mathrm{p2p}} - C_{\mathrm{VPP}i}^{\mathrm{coo}}\right)\right] + \sum_{i=1,i\neq j}^{n}\sum_{j=1}^{n}\sum_{t=1}^{T}\Big[\chi_{t,e}^{i,j}\left(p_{i,j,e,t} - p_{j,i,e,t}\right) + \chi_{t,h}^{i,j}\left(p_{i,j,h,t} - p_{j,i,h,t}\right) + \Big] + \sum_{i=1,i\neq j}^{n}\sum_{j=1}^{n}\sum_{t=1}^{T}\Big[\frac{\sigma_e}{2}\| p_{i,j,e,t} - p_{j,i,e,t} \|_2^2 + \frac{\sigma_h}{2}\| p_{i,j,h,t} - p_{j,i,h,t} \|_2^2\Big]\Bigg\} \tag{32}$$

where

$$\pi \in \Big\{P_{t,\mathrm{e}}^{\mathrm{buy}}, P_{t,\mathrm{e}}^{\mathrm{sell}}, P_{t,\mathrm{e}}^{\mathrm{CHP}}, P_t^{\mathrm{dis}}, P_t^{\mathrm{chr}}, P_{t,\mathrm{e}}^{\mathrm{cut}}, P_{t,\mathrm{e}}^{\mathrm{sl}}, P_{t,\mathrm{pv}}^{\mathrm{VPPO,real}}, P_{t,\mathrm{wt}}^{\mathrm{VPPO,real}}, P_{t,\mathrm{e}}^{\mathrm{load,reai}}, P_{t,\mathrm{h}}^{\mathrm{load,reai}}, P_{t,\mathrm{e}}^{\mathrm{buy}}, P_{t,\mathrm{e}}^{\mathrm{sell}}, P_{t,\mathrm{e}}^{\mathrm{CHP}}, P_t^{\mathrm{dis}}, P_t^{\mathrm{chr}}, P_{t,\mathrm{h}}^{\mathrm{cut}}, P_{t,\mathrm{h}}^{\mathrm{sl}}, P_{i,j,e,t}^{\mathrm{P2P}}, P_{i,j,h,t}^{\mathrm{P2P}}\Big\}$$

$\lambda_{t,\mathrm{e}}^{i,j}$ $\lambda_{t,\mathrm{h}}^{i,j}$ represent the Lagrange multiplier and $\xi_e \xi_{\mathrm{h}}$ represent the penalty factor. For the VPP i, the expected energy interaction of the remaining VPP j is received, and then the distributed optimization model of the VPP i is solved to obtain the expected energy interaction of the VPP i. Next, the number of iterations of the ADMM algorithm is increased by 1 and the dual variables are updated to determine the convergence of the ADMM algorithm. If it is less than the convergence accuracy ε, convergence stops:

$$\begin{cases} \sum_{j=i,j\neq i}^{n}\sum_{t=1}^{\mathrm{T}} \| P_{i,j,e,t}^{\mathrm{P2P}} + P_{j,i,e,t}^{\mathrm{P2P}} \| \leq \varepsilon \\ \sum_{j=i,j\neq i}^{n}\sum_{t=1}^{\mathrm{T}} \| P_{i,j,h,t}^{\mathrm{P2P}} + P_{j,i,h,t}^{\mathrm{P2P}} \| \leq \varepsilon \end{cases} \tag{33}$$

Similarly, the augmented Lagrange function for constructing the SP2 is as follows:

$$L_i^{\mathrm{SP2}}\left(p_{i,j,e,t}, p_{i,j,h,t}\right) = \min\Bigg\{-\ln\left[\left(C_{\mathrm{VPP}i}^{\mathrm{non}} - C_{\mathrm{VPP}i}^{\mathrm{p2p}} - C_{\mathrm{VPP}i}^{\mathrm{coo}}\right)\right] + \sum_{i=1,i\neq j}^{n}\sum_{j=1}^{n}\sum_{t=1}^{T}\Big[\chi_{t,e}^{i,j}\left(p_{i,j,e,t} - p_{j,i,e,t}\right) + \chi_{t,h}^{i,j}\left(p_{i,j,h,t} - p_{j,i,h,t}\right) + \Big] + \sum_{i=1,i\neq j}^{n}\sum_{j=1}^{n}\sum_{t=1}^{T}\Big[\frac{\sigma_e}{2}\| p_{i,j,e,t} - p_{j,i,e,t} \|_2^2 + \frac{\sigma_h}{2}\| p_{i,j,h,t} - p_{j,i,h,t} \|_2^2\Big]\Bigg\} \tag{34}$$

where $\chi_{t,e}^{i,j}\chi_{t,h}^{i,j}$ represent the Lagrange multiplier, and σ_e and σ_h are the penalty factors.

The ADMM distributed optimization is carried out with minimizing l as the objective function. In the iterative calculation process of the same SP1, the algorithm convergent after satisfying the following formula.

$$\begin{cases} \sum_{j=i,j\neq i}^{n}\sum_{t=1}^{T} \| p_{i,j,e,t} - p_{j,i,e,t} \| \leq \varepsilon \\ \sum_{j=i,j\neq i}^{n}\sum_{t=1}^{T} \| p_{i,j,h,t} - p_{j,i,h,t} \| \leq \varepsilon \end{cases} \tag{35}$$

Therefore, the Nash bargaining model is decomposed into the VPP cost minimization SP1 and the VPP revenue distribution SP2. Coupling constraints are set and the augmented Lagrangian functions of each problem are established. The ADMM method is adopted for distributed solution. The specific solution process of the Nash-Stackelberg game is shown in Fig. 3.

The ADMM method can only directly handle a single interaction quantity at a time. However, in this paper, the electricity price and electricity energy interaction quantities exist in two separate solution problems (SP1 and SP2), so ADMM is used for separate processing in each sub-problem. To sum up, the Nash-Stackelberg game model framework with multiple uncertainties proposed in this paper is divided into three parts. Solving the Stackelberg game part, that is, solving the breakdown point of the Nash bargaining, and solving the Nash bargaining SP1 and SP2. The final output is the breakdown point of the Nash bargaining, namely the independent operating cost, the interaction volume of the electric heating P2P in SP1 and the cost after participating in P2P, the transaction price of the electric thermal P2P in SP2, and the benefit of the Nash bargaining.

3.4 Nash-Stackelberg game model and convergence analysis of ADMM algorithm

To prove that the Nash-Stackelberg model in this paper has a unique optimal solution, based on the four axiomatic conditions proposed by Nash [25]: Pareto efficiency, symmetry, invariance to affine transformations, and independence of irrelevant alternatives. When the Nash bargaining solution satisfies these four conditions, it is the optimal solution [26,27]. The detailed proof process can be found in Appendix D.

For the Nash-Stackelberg game framework, this paper uses the standard ADMM for distributed solution. However, in the case of three/multi-block, its convergence cannot be guaranteed [28,29]. In the Nash-Stackelberg model of this paper, the three VPPs act as the game entities, and their objective functions, constraint conditions, and decision variables have the same form. From the perspective

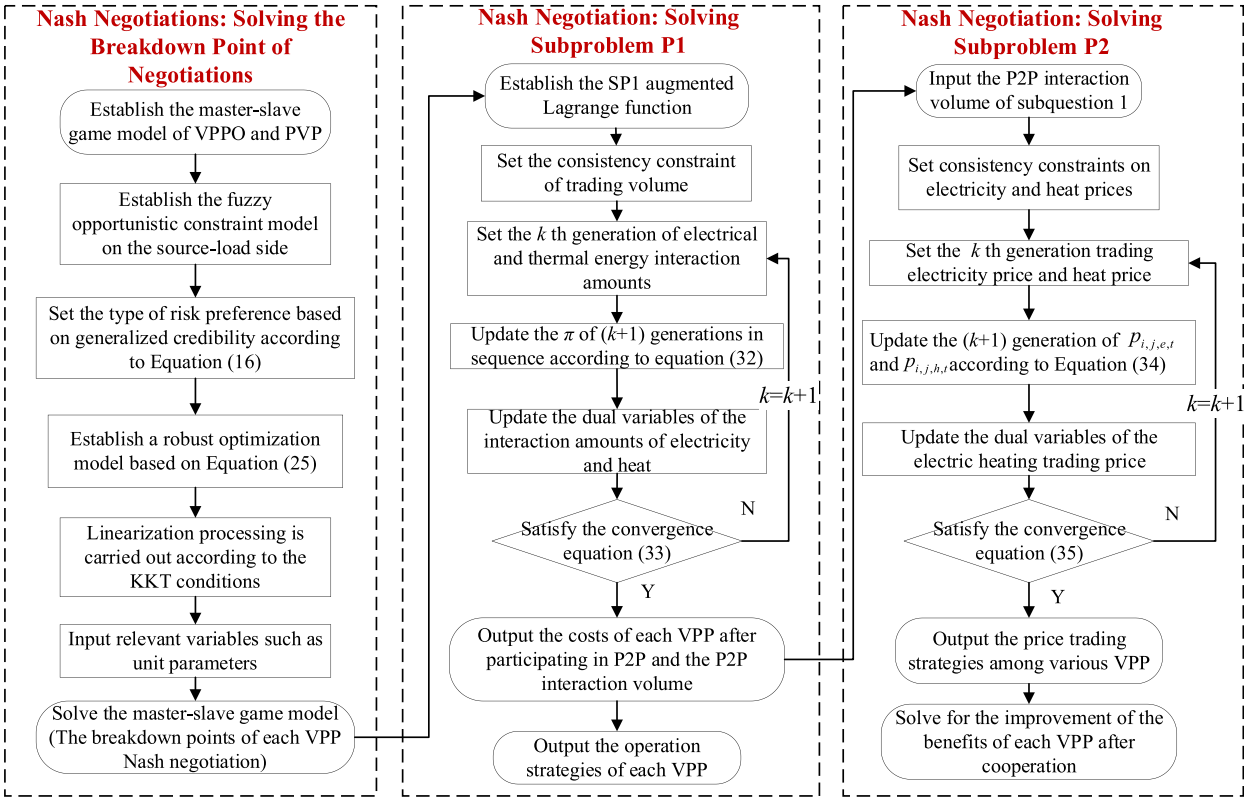

Fig. 3. The solution process of the Nash-Stackelberg game mod.

of the type of the mathematical programming model, The optimization problems of VPP operation all fall under the category of mixed-integer linear programming problems, with only the parameters varying among different entities, so they belong to the one block of problem [30], and can be solved by the standard ADMM for distributed computation.

Existing literature indicates that when the dimension of integer variables is small, ADMM can achieve better convergence [23]. However, when a large number of integer variables are large in scale, the model shows strong non-convexity, and the standard ADMM cannot directly converge. At this time, it is necessary to combine the Alternating Optimization and Projection(AOP) algorithm. First, continuous relaxation is performed on the integer variables to solve, and then the feasible integer solution is gradually approximated through projection and iterative methods, thereby ensuring convergence [31].

4 Case analysis

4.1 Parameter Settings

The numerical examples in this article are three VPP systems, The data structure of the unit is based on reference [23] and has been adjusted accordingly. The relevant parameters are shown in Appendix E. All simulations are conducted in the MATLAB 2021b in a 64-bit Windows environment with Cplex 12.7.0 solver and YALMIP toolbox on a PC with Core i7-12700 CPU @1.8 GHz and 16 GB RAM. Programming was carried out using Matlab. The convergence accuracy of the ADMM algorithm was set to 10^{-3} and the penalty factor was 10^{-3}. Set the confidence level of the fuzzy chance constraint at 90%; During the high-risk period, take the time points corresponding to the 12 data with larger absolute values of source charges; during the low-risk period, take the time points corresponding to the 12 data with smaller absolute values of source charges. Set the initial β_t ($t \in c$, $c = 1$) to 0.6 and β_t ($t \in c$, $c = 2$) to 0.4; The fluctuation $\varphi_e \varphi_h$ of electricity and thermal prices is taken as 10% [32], and the initial setting of the uncertainty period Γ is 15.

4.2 Analysis of game economic benefits

Four different scene are set up to analyze the effectiveness of the Nash-Stackelberg game optimization operation established in this paper under multiple uncertainty scene. Among them, scene 3 is the traditional clear equivalence class. Scene 4 represents the traditional random optimization method. Considering the uncertainty of wind and solar power output, 1000 scenes were generated using Latin hypercube sampling, and 5 typical scenes were obtained using the backward reduction method [14]. Scene 5 is the clear equivalence class based on generalized credibility proposed in this paper. The scene Settings are shown in Table 3.

First, take Scene 5 as an example. The convergence of the algorithm before and after the Nash-Stackelberg game is shown in Fig. 4.

Fig. 4 illustrates that following the distributed solution via ADMM, SP1 converges 35 times, with convergence accuracies for electrical energy and thermal energy recorded at 4.8634×10^{-5} and 5.7067×10^{-11}, respectively. SP2 converges 33 times, with convergence accuracies for electrical energy and thermal energy recorded at 1.8240×10^{-5} and 8.3523×10^{-5}, respectively. Both satisfy the criteria for convergence. Therefore, the proposed ADMM algorithm ensures robust convergence, model stability, privacy protection for all VPPs, and fulfillment of Nash bargaining criteria.

Then calculate the independent operation of each VPP and the cost after Nash bargaining in the Nash-Stackelberg game. The comparison of the benefit analysis of the Nash-Stackelberg game in scene 1 to 5 is shown in Table 4, where the cost reduction amplitude is the proportion of the cost change amount after Nash bargaining to the total cost during independent operation.

Table 4 shows that scene 2 alone compensates for pricing uncertainty due to a more conservative strategy, increasing the ultimate cost of Nash bargaining inside the VPP association by 6707.79 CNY. The VPP topic partially relaxes the fuzzy opportunity restriction, making the equivalence class predictable. This decision-making space extension increases P2P and Nash bargaining efficiency costs while reducing uncertainty losses and improving system security. In a conservative strategy with broad confidence, the conservative approach during high-risk periods handles more risk factors than the optimistic strategy during low-risk periods. So, high-risk times cost more than low-risk periods, totaling 69.15 CNY per scene under the Nash bargaining framework. VPP1′s Nash bargaining benefits grew from 1320.79 to 1331.07 CNY uncertain conditions. After compensating for their own mistakes, the VPP reduced transactions with the external grid and thermal network and traded with its own VPP. Scene4 has a total cost that is equal to the expected cost, which is slightly higher than the cost in Scene 2 of the deterministic optimization of new energy output. This is mainly because the stochastic optimization calculates different scenes of

Table 3
The setting of uncertain scene in the Nash-Stackelberg game.

Scene	Uncertainty of source and charge	uncertainty of electricity and thermal prices
Scene 1	×	×
Scene 2	×	√
Scene 3	√ (Tradition)	√
Scene 4	√ ([14])	√
Scene 5	√ (Article)	√

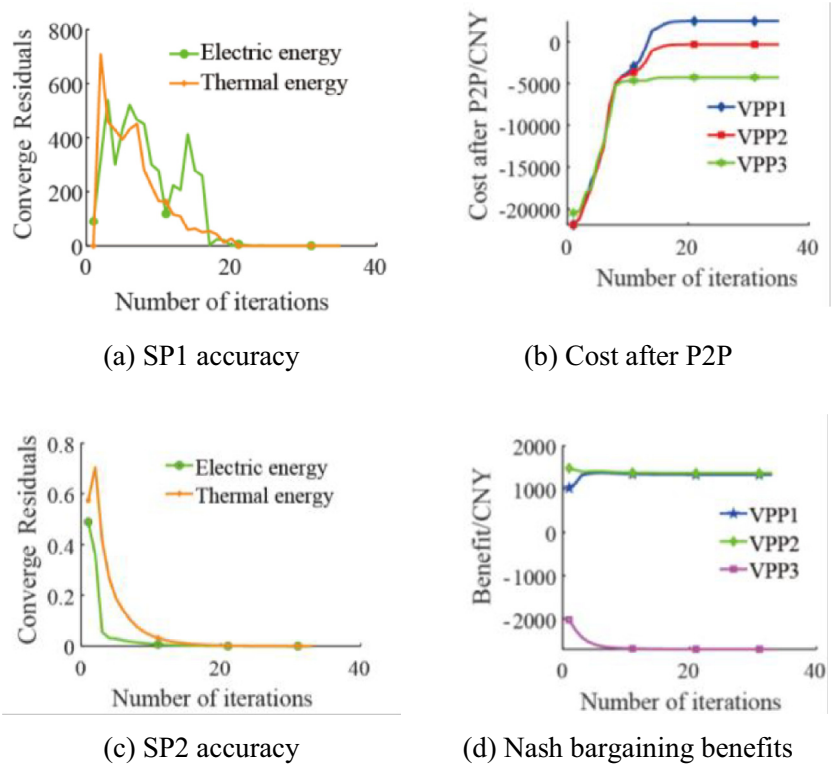

(a) SP1 accuracy (b) Cost after P2P

(c) SP2 accuracy (d) Nash bargaining benefits

Fig. 4. Scene 4 ADMM iteration process.

Table 4
Benefit analysis of the Nash-Stackelberg game in different scenes (unit: CNY).

Scene	Subject	Cost of independent operation	Cost after participating in P2P	Nash bargaining benefits	Final cost of Nash bargaining	Cost reduction amplitude (%)
Scene 1	VPP1	−7140.77	−6196.70	1320.79	−7517.49	5.28%
	VPP2	−10440.14	−9668.80	1148.05	−10816.85	3.61%
	VPP3	−9156.46	−12001.89	−2468.73	−9533.17	4.11%
Scene 2	VPP1	−4977.37	−4257.27	980.76	−5238.03	5.24%
	VPP2	−8221.05	−7175.27	1306.42	−8481.69	3.17%
	VPP3	−7179.36	−9727.07	−2287.07	−7440.00	3.63%
Scene 3	VPP1	1406.24	2396.41	1336.20	1060.22	24.61%
	VPP2	−1381.75	−353.09	1374.66	−1727.76	25.04%
	VPP3	−1258.72	−4315.47	−2710.75	−1604.72	27.49%
Scene 4	VPP1	−3943.8237	−3330.8928	899.3974	−4230.2901	7.26%
	VPP2	−7172.6513	−5764.1932	1694.9021	−7459.0953	3.99%
	VPP3	−5974.0417	−8854.6694	−2594.1817	−6260.4878	4.79%
Scene 5	VPP1	1431.66	2414.65	1331.07	1083.58	24.31%
	VPP2	−1348.95	−333.72	1363.31	−1697.03	25.80%
	VPP3	−1241.56	−4282.87	−2693.20	−1589.67	28.04%

new energy output separately and needs to simultaneously meet the operation scheduling plans under different typical scenes. Therefore, it exchanges certain economic benefits for the robustness of the optimized scheduling strategy. Nash's P2P trading process benefits from VPP1 and VPP2, with scene 3, 4 and 5 outperforming scenes 1 and 2. Robust optimization and stochastic optimization P2P transactions within the cooperative game, making it more suitable for multi-agent collaboration in complex and uncertain environments.

Furthermore, when solving Nash bargaining SP1, the computing time and power exchange amount of the solution were compared between the calculation using the centralized algorithm and the calculation using the ADMM algorithm. The results are shown in Table 5 and Fig. 5.

From Table 5 and Fig. 5, the centralized algorithm outperforms the distributed one in solution time. This is because it processes all data centrally, enabling fast acquisition of the global optimal solution—whereas the distributed algorithm requires communication and iteration across multiple nodes. In terms of power interaction, the power exchange volume solved by the centralized algorithm fluctuates significantly, while the distributed algorithm yields a smoother interaction curve. This is attributed to the distributed algorithm's iterative optimal solution search and its allowance for each VPP to make independent decisions based on its own conditions, thereby reducing impacts on other VPPs.

In conclusion, although the centralized algorithm has certain advantages in terms of solution speed, in actual operation, the fluctuation of interaction volume can cause problems such as equipment lifespan reduction. However, the distributed algorithm results in a smaller fluctuation in the power interaction volume, which has stability and is more suitable for actual operation scenes. Moreover, each VPP can make independent decisions without sharing all the data, which can protect the privacy of the VPP.

4.3 Analysis of game operation strategies

To verify the feasibility and effectiveness of the Nash-Stackelberg game model proposed in this paper, three game strategies were compared. The results are shown in Table 7:

Table 5
Comparison of solving time for different algorithms (unit: second).

	Centralize	ADMM
Time	1.40	22.83

1) Strategy 1: Takes into account both the Stackelberg game and the Nash cooperation game among each VPP, which is the scene 5 set in this paper.
2) Strategy 2: Only considers the Stackelberg game but does not consider the Nash cooperation game among VPP.
3) Strategy 3: Does not consider the Stackelberg game, and fixes the electricity and heat prices for the lower-level PVP. The obtained lower-level optimal response is taken as a known quantity and substituted into the upper level, while considering the cooperation game among each VPP.

As shown in Table 6, in the method of this paper, the VPP conducts a master–slave game internally. Compared with the fixed electricity price, it can ensure that the upper and lower-level entities in the game process aim to minimize their own costs, dynamically optimize the transaction price and purchase quantity between VPPO and PVP, and ultimately achieve the minimum total cost of the VPP as a whole. Further, VPPs engage in cooperative games, achieving the optimal benefit of the VPP alliance through P2P transactions of electricity and heat, resulting in a final cost that is 1044.27 CNY lower than Strategy 2 and 4357.08 CNY lower than Strategy 3.

4.4 Analysis of game operation strategies

After the Nash bargaining, each entity has more abundant resources to dispatch after joining the P2P electric thermal trading. While the leader fully consumes wind power and photovoltaic power, the VPP entities obtain additional benefits through P2P. The dispatching result of the electric heating load of VPP1 in Scene 5 is shown in Fig. 6.

Fig. 6 illustrates that, regarding the power balance of the electricity load, during peak electricity purchase price periods from the external power grid, specifically between 11:00 and 15:00, the dispatching strategy is selected to facilitate P2P transactions with VPP2 and VPP3 to reduce electricity purchase costs. When the photovoltaic power is

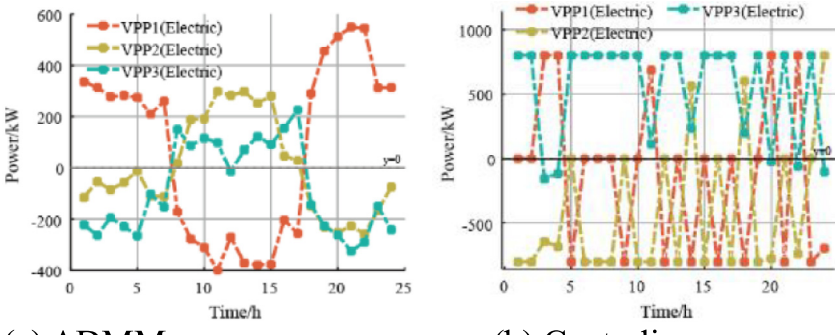

(a) ADMM (b) Centralize

Fig. 5. Comparison of SP1 Electric interaction.

Table 6
Cost comparison under different game strategies (unit: CNY).

Strategy	VPP	Stackelberg	Nash bargaining benefits	Total cost
1	1	1431.66	1331.07	−2203.12
	2	−1348.95	1363.31	
	3	−1241.56	−2693.20	
2	1	1431.66	0	−1158.85
	2	−1348.95	0	
	3	−1241.56	0	
3	1	2871.28	1483.75	2153.96
	2	848.80	1259.65	
	3	–232.87	−2743.29	

Table 7
Fuzzy parameter setting in the Nash-Stackelberg game.

Level	η_1	η_2	η_3	η_4
Fuzzy level 1	0.85	0.95	1.05	1.15
Fuzzy level 2	0.8	0.9	1.1	1.2

little at night, it opts not to procure electricity directly from the external power grid to maintain its power balance. CHP units receive preferential access to power supply, and surplus electricity is marketed through P2P transactions to generate supplementary income. During the off-peak period for electricity pricing, the transaction price of P2P exceeds the cost of procuring electricity from the external power grid. Consequently, procuring electricity from the external grid is prioritized. From the standpoint of thermal load power equilibrium, the majority of thermal power is supplied by GB. From 8:00 to 12:00 in the morning, the thermal load demand is comparatively low, representing the nadir of the thermal purchase price. Concurrently, the supplementary acquired thermal energy is exchanged via P2P to capitalize on the price differential. During the peak thermal pricing time, the thermal balancing P2P transaction price and the upward heating price facilitate flexible thermal energy trading. Reduce personal operational expenses.

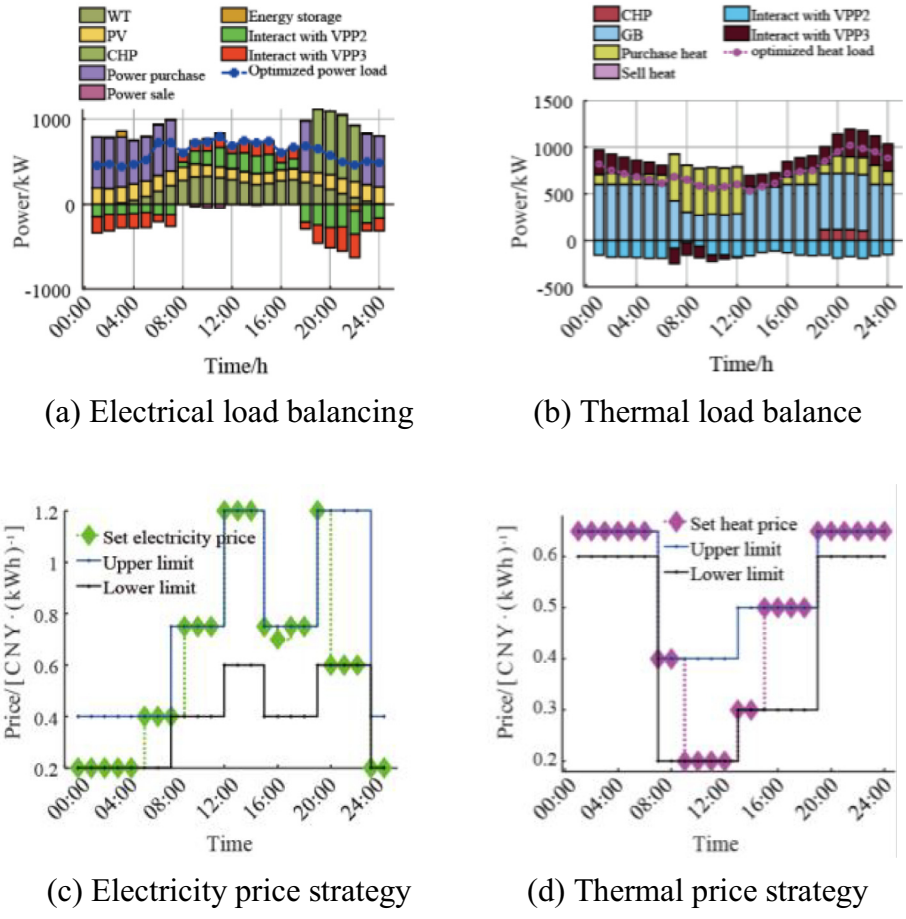

(a) Electrical load balancing (b) Thermal load balance

(c) Electricity price strategy (d) Thermal price strategy

Fig. 6. Scheduling results of VPP1 electric and heating load in different scenes.

4.5 Sensitivity analysis of uncertain parameters

This section conducts a sensitivity analysis of the relevant parameters in multiple uncertainties to verify the stability of the model. Firstly, the influence of the size of the trapezoidal fuzzy set on the result of the Nash-Stackelberg game is analyzed. The Settings of the fuzzy parameters are shown in Table 7.

The comparison of the penalty cost of price fluctuations and the final cost of Nash bargaining within different confidence intervals ($\alpha = 90\%$, $\alpha = 85\%$, $\alpha = 80\%$) under different fuzzy parameter Settings in Table 3 is shown in Fig. 7. fuzzy levels 1 takes into account the fluctuation range of 85–115% of the source charge, while fuzzy levels 2 further relaxes the trapezoidal ambiguity set, with a fluctuation range between 80% and 120%.

Fig. 7 demonstrates that although fuzzy level 2 incorporates additional risks, penalty costs for price fluctuations remain relatively stable across ambiguity levels. The Nash-Stackelberg framework effectively mitigates price fluctuation penalties induced by heightened uncertainty. By consolidating resources and benefits across VPPs, the system tolerates a broader range of source charge uncertainty parameters without substantially increasing price fluctuation penalties. As α increases, the VPP system accommodates more uncertainty variables, relaxing source-load constraints and requiring additional thermal/-electrical loads to maintain power balance. This consequently degrades economic performance. When ambiguity escalates (trapezoidal uncertainty parameter: 80–120%), VPP risk exposure increases, reducing the final Nash bargaining cost. Therefore, optimal confidence levels should be carefully selected through comprehensive risk-economic trade off analysis according to system-specific requirements.

To further explore the influence on the economic benefits of the Nash-Stackelberg game under different types of risk preference, the Settings of different risk preference types are shown in Table 8. Taking the VPP1 system as an example, the comparison results are shown in Fig. 8.

Fig. 8 demonstrates that source-load risk preferences during high-risk and low-risk periods influence the optimization method. This study classifies high-risk data as conservative and low-risk data as optimistic, reflecting operational aspects of the VPP in response to temporal variations in source-load risk sensitivity. During the high-risk phase, analysis of the conservative type reveals an increase in source-load risk variables, as indicated in Table 9. Under these conditions, the upper-right endpoint weight $[\alpha - (1 - \beta_c) / \beta_c]$ exceeds $(2\alpha\text{-}1)$. Consequently, the upper-limit risk of the trapezoidal fuzzy parameter is considered. For the optimistic risk preference (type 3), the independent operational cost and Nash bargaining cost exceed 1214.54 CNY and 872.39 CNY, respectively, during high-risk and low-risk periods. The optimistic type's preference for source-load risk may stem from a lower perceived risk, as the associated cost reduction is minimized at

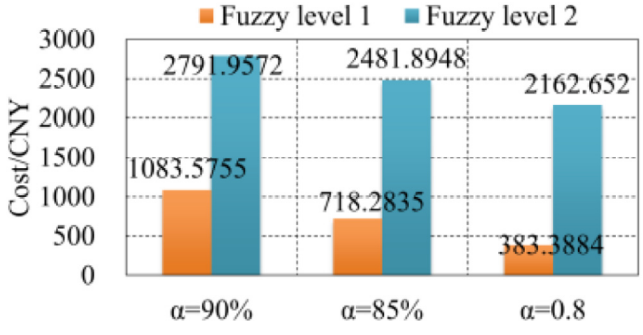

(a) Price fluctuations penalize costs

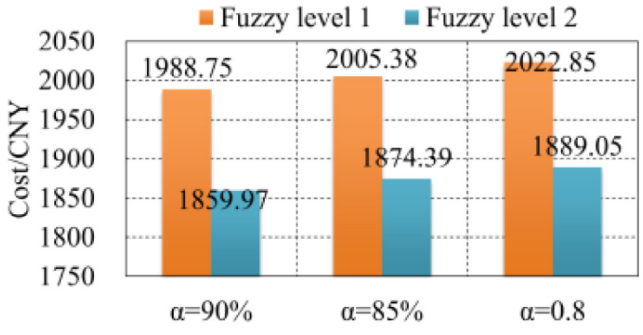

(b) Final cost of nash bargaining

Fig. 7. Comparison under different fuzzy levels.

Table 8
Parameter settings for different risk preference types.

Risk preference type	β_t ($t \in c$)	
	High risk period(c = 1)	Low risk period(c = 2)
Type 1	0.6(Conservative)	0.4(Optimistic)
Type 2	0.8(Conservative)	0.4(Optimistic)
Type 3	0.4(Optimistic)	0.4(Optimistic)
Type 4	0.6(Conservative)	0.6(Conservative)
Type 5	0.9(Conservative)	0.9(Conservative)

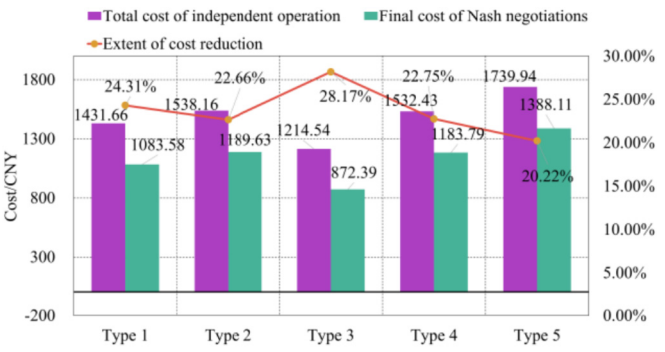

Fig. 8. Comparison under different levels of risk preference.

Table 9
Analysis of model optimization results under different scale VPPs.

VPP numbers	Overall cooperative revenue of VPP /CNY	SP1 Iterative Convergence Count	Running time of SP1 program/s
5	6261.43	34	39.19
10	8250.76	68	172.35
15	12109.52	75	463.20
20	18647.73	91	2423.68

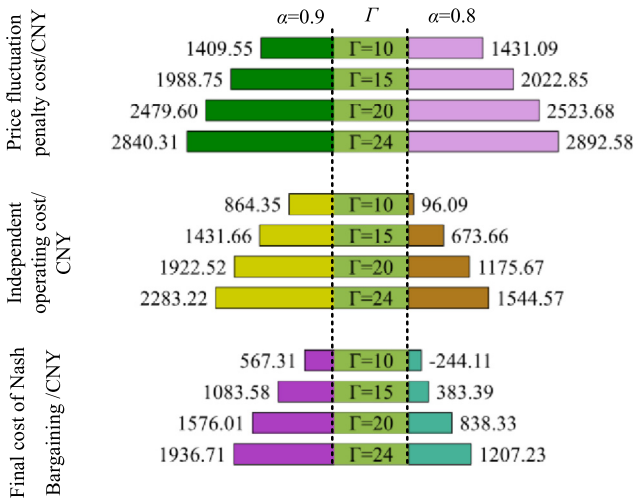

Fig. 9. Cost comparison during uncertain periods.

28.17%. This strategy reduces costs and benefits the partnership. During the high-risk phase, risk preference type 2 exhibits a higher β_c than type 1, resulting in an overall cost increase of 104.5 CNY before and 106.05 CNY after the final Nash bargaining. Similarly, in the high-risk period, risk preference type 5 has a higher β_c than type 4. This leads to increases in the final Nash bargaining costs of 207.51 CNY and 204.32 CNY, respectively. Relative to type 1, this heightened risk during low-risk periods increases independent operation costs by 7.04% and Nash bargaining costs by 9.25%.

The comparison results of the model's price fluctuation penalty cost and the various costs of the Nash-Stackelberg game at different confidence intervals ($\alpha = 0.9$ and $\alpha = 0.8$) under different uncertainty periods ($\Gamma = 10, 15, 20, 24$) are shown in Fig. 9.

Fig. 9 demonstrates that decreasing α increases the probability of constraint violations. Under these conditions, greater weights should be assigned to the left and right endpoints of the trapezoidal fuzzy parameter's upper base (closer to the central value), thereby permitting more frequent constraint violations. Reserves for excessive price fluctuation penalties are required to improve constraint satisfaction probability. Consequently, both price fluctuation penalty costs and post-P2P transaction costs increase. As the uncertainty period Γ extends, more time intervals incorporate thermal fluctuation-induced uncertainty costs, resulting in persistent increases to both the model's price fluctuation penalty costs and the final Nash bargaining

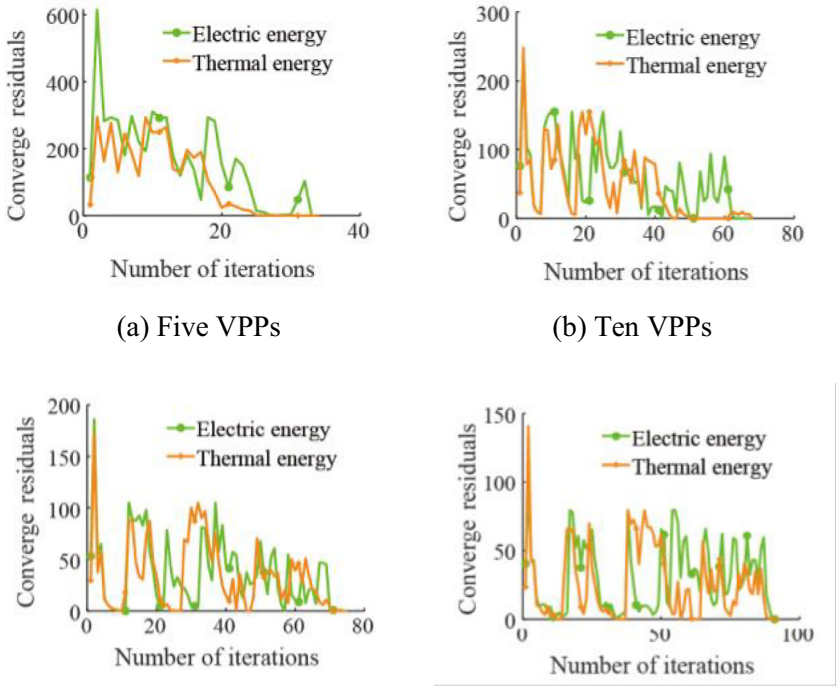

Fig. 10. Convergence residuals of ADMM under different scale VPPs.

cost. The latter also exhibits heightened uncertainty risks due to increasing Γ and decreasing α. When $\Gamma = 24$ (accounting for power and heat cost variations across all dispatching cycles), the final Nash bargaining cost reaches its maximum. Furthermore, reducing α signifies that in higher-uncertainty environments, the model prioritizes source charge sensitivity across time intervals: augmenting weight η_3 for high-risk periods and η_2 for low-risk periods, while addressing fuzzy parameter risks in sensitive intervals.

4.6 Research on the main computational bottleneck of large-scale VPP

To further evaluate the effectiveness of the proposed method in a large-scale environment, we conducted verification analyses on test systems with 5, 10, 15, and 20 multiple VPP entities [24,33]. The example results are as follows.

From Table 9, it can be seen that for the examples of different VPP entities, the method proposed in this paper can achieve effective convergence within a limited number of iterations. The specific residual convergence curves are shown in Fig. 10. Moreover, the program running time of the proposed method can also meet the actual requirements of real-time operation scheduling. It should be particularly noted that the simulation platform constructed in this paper is a single-computer environment, while ADMM itself has the characteristic of distributed optimization. If it is deployed in a parallel computing environment, the overall program running time can be significantly shortened. At the same time, as the number of VPP participating entities increases, the overall cooperative revenue of the VPP alliance shows an increasing trend, which indicates the feasibility of the proposed model in large-scale test systems.

5 Conclusion

This paper addresses collaborative optimization of VPPs under uncertainty through a multi-faceted uncertainty modeling framework integrating enhanced fuzzy chance constraints with robust optimization. A Nash-Stackelberg game-theoretic model is developed to facilitate VPP coalition operations and maximize alliance benefits. Results demonstrate that the proposed framework significantly reduces operating costs for both VPPO and PVP while minimizing total alliance expenditures and optimizing benefit distribution. The enhanced fuzzy chance constraint model—based on generalized credibility—generates risk-preferential operational strategies across high/low-risk periods, overcoming traditional methods' limitations in temporal risk differentiation. Concurrently, the robust optimization component enhances VPPs' resilience against electricity price volatility during collaboration, adaptively regulating risk exposure according to price fluctuation frequency. Future research directions could further consider using joint probability distributions or distributionally robust optimization to describe the correlation between sources, loads and prices, and construct a joint uncertainty set to provide more refined risk control strategies for practical engineering. At the same time, when dealing with the three/multi-block problem, it is also necessary to design an innovative distributed solution algorithm.

It should be noted that the Nash-Stackelberg hybrid game model proposed in this paper is not merely at the theoretical level; instead, it directly addresses the actual needs of more than ten VPPs and operators that have been in operation in places like Suqian and Nanjing. Currently, these operators generally adopt a simplified model of hierarchical game, and the current day-ahead contract electricity volume and price mainly rely on manual experience, lacking quantitative bargaining tools. In future research, the implementation of dynamic pricing strategies and Nash bargaining strategies can be further explored.

CRediT authorship contribution statement

Lei Dong: Methodology, Funding acquisition. **Shuaibo Zhang:** Writing – original draft, Software, Data curation. **Yang Li:** Project administration, Methodology. **Zibo Wang:** Writing – review & editing, Conceptualization. **Binwen Zhang:** Data curation. **Hong Zhu:** Writing – review & editing, Funding acquisition. **Wenlu Ji:** Resources, Methodology.

Declaration of competing interest

The authors declare the following financial interests/personal relationships which may be considered as potential competing interests: Yang LI, Zibo WANG and Binwen ZHANG are currently employed by China Electric Power Research Institute; Hong ZHU and Wenlu JI are currently employed by State Grid Jiangsu Electric Power Co., Ltd.

Acknowledgments

This work was supported by Science and Technology Project of SGCC (Research on Distributed Cooperative Control of Virtual Power Plants Based on Hybrid Game) (5700-202418337A-2-1-ZX).

Appendix A

Theorem 1. The credibility of the fuzzy event $g\left(x,\widetilde{P}\right)$ is defined as:

$$\mathrm{Cr}\left\{g\left(x,\widetilde{P}\right)\le 0\right\}=\tfrac{1}{2}\left[Poss\left\{g\left(x,\widetilde{P}\right)\le 0\right\}+Nec\left\{g\left(x,\widetilde{P}\right)\le 0\right\}\right] \tag{A1}$$

where $Poss\{A\}=sup\mu_{\widetilde{P}}(x)$ represents the maximum possibility of the event occurring, and $\mathrm{Nec}\{A\}=1-\mathrm{Poss}\{A\}$ represents the minimum possibility of the event not occurring.

Theorem 2. When $\alpha \ge 0.5$, there is a clear equivalence class formula for symmetrical trapezoids:

$$\begin{aligned}&(2-2\alpha)\sum_{m=1}^{M}\left(R_{m,3}h_m^{+}(\boldsymbol{x})-R_{m,2}h_m^{-}(\boldsymbol{x})\right)+\\&(2\alpha-1)\sum_{m=1}^{M}\left(R_{m,4}h_m^{+}(\boldsymbol{x})-R_{m,1}h_m^{-}(\boldsymbol{x})\right)+h_0(\boldsymbol{x})\le 0\end{aligned} \tag{A2}$$

where m is a fuzzy variable (m = 1,2,... M), $h_m^{+}(\boldsymbol{x})$ and h_m^{-} respectively have the m value being positive or negative, which are fuzzy variables, and $h_0(\boldsymbol{x})$ is the descending part of the non-trapezoidal fuzzy set.

From Theorem 1, it can be known that based on the symmetrical trapezoid ($\eta_2-\eta_1=\eta_4-\eta_3=\Delta r$), the membership degree of the left ascending segment is $\mu_{\mathrm{L}}=\frac{x-\eta_1}{\Delta r}(x\in[\eta_1,\eta_2])$: The membership degree of the right descending segment is $\mu_{\mathrm{R}}=\frac{\eta_4-x}{\Delta r}(x\in[\eta_3,\eta_4])$.

According to the credibility requirement that $Cr\ge\alpha$, in order to convert the nonlinear membership degree into linear constraints, the weights w_{L} and w_{R} are defined to amplify the influence of the left and right segments respectively, making them satisfy $w_{\mathrm{L}}\cdot\mu_{\mathrm{L}}+w_{\mathrm{R}}\cdot\mu_{\mathrm{R}}\ge\alpha$. Combined with the normalization condition of the symmetrical trapezoid, it is finally derived that w_{L}= (2-2α) and w_{R} = (2α-1). On this basis, based on generalized credibility, there are:

$$\begin{aligned}\mathrm{Cr}\left\{g\left(x,\widetilde{P}\right)\le 0\right\}=\beta_t\cdot\mathrm{Poss}\left\{g\left(x,\widetilde{P}\right)\le 0\right\}+\\(1-\beta_t)\cdot\mathrm{Nec}\left\{g\left(x,\widetilde{P}\right)\le 0\right\}\end{aligned} \tag{A3}$$

where, $\beta_t\in[0,1]$ is the risk preference parameter.

In the right descending segment, the credibility of the trapezoidal fuzzy set is:

$$\begin{aligned}&\Rightarrow x=\eta_3+(\eta_4-\eta_3)\tfrac{\alpha-(1-\beta_t)}{\beta_t}\\&\Rightarrow x-\eta_3=\tfrac{\eta_4-\eta_3}{\beta_t}(\alpha-(1-\beta_t))\\&\Rightarrow x=\eta_3+\tfrac{\eta_4-\eta_3}{\beta_t}(\alpha-(1-\beta_t))\\&\Rightarrow x=\left(1-\tfrac{\alpha-(1-\beta_t)}{\beta_t}\right)\eta_3+\tfrac{\alpha-(1-\beta_t)}{\beta_t}\eta_4\end{aligned} \tag{A4}$$

Therefore, the weight of η_4 is obtained as $\frac{1-\alpha}{\beta_t}$; The weight of η_3 is $\frac{\alpha-(1-\beta_t)}{\beta_t}$.

The independence of different risk levels is reflected in the fact that the sets of time periods they cover have no intersections (are mutually exclusive), and their respective parameters are independently set.

Appendix B

The Lagrange function constructed based on dual variables is:

$$\begin{aligned}\underset{\varsigma_1,\varsigma_2,\varsigma_3,\varsigma_4}{L}=&\sum_{c=1}^{C}\sum_{t\in c}^{T_C}\left[\varphi_{\mathrm{e}}P_{t,\mathrm{e}}^{\mathrm{load,reai}}U_{t,\mathrm{e}}^{\varphi}+\varphi_{\mathrm{h}}P_{\mathrm{h,e}}^{\mathrm{load,reai}}U_{t,\mathrm{e}}^{\varphi}\right]+\\&\varsigma_1\left(\Gamma-\sum_{t=1}^{T}U_{t,\mathrm{e}}^{\varphi}\right)+\varsigma_2\left(\Gamma-\sum_{t=1}^{T}U_{t,\mathrm{h}}^{\varphi}\right)+\\&\varsigma_3\left(1-U_{t,\mathrm{e}}^{\varphi}\right)+\varsigma_4\left(1-U_{t,\mathrm{h}}^{\varphi}\right)\end{aligned} \tag{B1}$$

Final translation: Organized as follows:

$$\begin{aligned}&\sum_{c=1}^{C}\sum_{t\in c}^{T}\left(\varphi_{\mathrm{e}}P_{t,\mathrm{e}}^{\mathrm{load,reai}}-\varsigma_1-\varsigma_2-\varsigma_3-\varsigma_4\right)U_{t,\mathrm{e}}^{\varphi}+\\&\sum_{c=1}^{C}\sum_{t\in c}^{T}\left(\varphi_{\mathrm{h}}P_{t,\mathrm{h}}^{\mathrm{load,reai}}-\varsigma_1-\varsigma_2-\varsigma_3-\varsigma_4\right)U_{t,\mathrm{h}}^{\varphi}+\\&\varsigma_1\Gamma+\varsigma_2\Gamma+\varsigma_3+\varsigma_4\end{aligned} \tag{B2}$$

When deriving the dual problem, first find the Lagrange function $\min\limits_{\varsigma_1,\varsigma_2,\varsigma_3,\varsigma_4} L$. Since the coefficients of $U_{t,\mathrm{e}}^{\varphi}$ and $U_{t,\mathrm{h}}^{\varphi}$ are $\left(\varphi_{\mathrm{e}}P_{t,\mathrm{e}}^{\mathrm{load,reai}}-\varsigma_1-\varsigma_2-\varsigma_3-\varsigma_4\right)$ and $\left(\varphi_h P_{t,h}^{load,reai}-\varsigma_1-\varsigma_2-\varsigma_3-\varsigma_4\right)$, and $0\le U_{t,e}^{\varphi},U_{t,h}^{\varphi}\le 1$. So when the coefficient is 0, $\min_{z_0} L(z_0,x_0,y_0,y_1)$ is obtained at $U_{t,e}^{\varphi},U_{t,h}^{\varphi}=0$.

In order to eliminate the nonlinear terms of $\varphi_{\mathrm{e}}P_{t,\mathrm{e}}^{\mathrm{load,reai}}$ and $\varphi_{\mathrm{h}}P_{t,\mathrm{h}}^{\mathrm{load,reai}}$ in the original max problem, auxiliary variables are introduced to transform the complex min–max problem into a linear optimization problem that is easier to solve. Linear constraints $-\widehat{P}_{\mathrm{e},0}\le P_{t,\mathrm{e}}^{\mathrm{load,reai}}\le\widehat{P}_{\mathrm{e},0}$ and $-\widehat{P}_{\mathrm{h},0}\le P_{t,\mathrm{h}}^{\mathrm{load,reai}}\le\widehat{P}_{\mathrm{h},0}$ are added, and$\widehat{P}_{\mathrm{e},0}\widehat{P}_{h,0}\ge 0$ are satisfied.

Meanwhile, to ensure the equivalent transformation, the dual problem is finally sorted out as:

$$\begin{cases}\min\sum_{t=1}^{T}(\varsigma_1\Gamma+\varsigma_2\Gamma+\varsigma_3+\varsigma_4)\\ s.t.\begin{cases}\varsigma_1+\varsigma_3\ge\varphi_{\mathrm{e}}\widehat{P}_{\mathrm{e},0},\varsigma_2+\varsigma_4\ge\varphi_{\mathrm{h}}\widehat{P}_{\mathrm{h},0}\\ -\widehat{P}_{\mathrm{e},0}\le P_{t,\mathrm{e}}^{\mathrm{load,reai}}\le\widehat{P}_{\mathrm{e},0}\\ -\widehat{P}_{\mathrm{h},0}\le P_{t,\mathrm{h}}^{\mathrm{load,reai}}\le\widehat{P}_{\mathrm{h},0}\\ \widehat{P}_{\mathrm{e},0}\ge 0,\widehat{P}_{h,0}\ge 0\\ \varsigma_1\ge 0,\varsigma_2\ge 0,\varsigma_3\ge 0,\varsigma_4\ge 0\end{cases}\end{cases} \tag{B3}$$

Appendix C

The Lagrangian function of the follower PVP model is:

$$
\begin{aligned}
&L\left(P_{t,\mathrm{e}}^{\mathrm{sl,in}}, P_{t,\mathrm{e}}^{\mathrm{sl,out}}, P_{t,\mathrm{e}}^{\mathrm{cut}}, P_{t,\mathrm{h}}^{\mathrm{cut}}, P_{t,\mathrm{wt}}^{\mathrm{real}}, P_{t,\mathrm{e}}^{\mathrm{load,reai}}, P_{t,\mathrm{h}}^{\mathrm{load,reai}}, \mu, \lambda\right) = \\
&\sum_{t=1}^{T}\left(p_{t,e}^{opt} P_{t,e}^{load,reai} + p_{t,\mathrm{h}}^{\mathrm{opt}} P_{t,\mathrm{h}}^{\mathrm{load,reai}}\right) + \sum_{t=1}^{T} P_{t,\mathrm{e}}^{\mathrm{cut}} f_{t,\mathrm{e}}^{\mathrm{cut}} + \sum_{t=1}^{T} P_{t,\mathrm{h}}^{\mathrm{cut}} f_{t,\mathrm{h}}^{\mathrm{cut}} + \\
&f_{\mathrm{pv}}^{\mathrm{dis}} \sum_{t=1}^{T}\left(P_{t,\mathrm{pv}}^{\mathrm{DPP}} - P_{t,\mathrm{pv}}^{\mathrm{DPP,real}}\right) + \mu_t^1\left(-P_{t,\mathrm{e}}^{\mathrm{cut}} + P_{\mathrm{min,e}}^{\mathrm{cut}}\right) + \\
&\mu_t^2\left(P_{t,\mathrm{e}}^{\mathrm{cut}} - P_{\mathrm{max,e}}^{\mathrm{cut}}\right) + \mu_t^3\left(-P_{t,\mathrm{h}}^{\mathrm{cut}} + P_{\mathrm{min,h}}^{\mathrm{cut}}\right) + \mu_t^4\left(P_{t,\mathrm{h}}^{\mathrm{cut}} - P_{\mathrm{max,h}}^{\mathrm{cut}}\right) + \\
&\mu_t^5\left(-P_{t,\mathrm{pv}}^{\mathrm{DPP,real}}\right) + \mu_t^6\left(P_{t,\mathrm{pv}}^{\mathrm{DPP,real}} - P_{t,\mathrm{pv}}^{\mathrm{DPP}}\right) + \\
&\lambda_t^1\left[P_{t,\mathrm{e}}^{\mathrm{Load}} - (2-2\alpha)P_{t,\mathrm{pv}}^{\mathrm{DPP,real}}\eta_2 - (2\alpha-1)P_{t,\mathrm{pv}}^{\mathrm{DPP,real}}\eta_1 - P_{t,\mathrm{e}}^{\mathrm{cut}} - \left(\tfrac{1-\alpha}{\beta_t}\eta_3 + \tfrac{\alpha-1+\beta_t}{\beta_t}\eta_4\right)P_{t,\mathrm{e}}^{\mathrm{load,reai}}\right] + \\
&\lambda_t^2\left[P_{t,\mathrm{h}}^{\mathrm{Load}} - P_{t,\mathrm{h}}^{\mathrm{cut}} - \left(\tfrac{1-\alpha}{\beta_t}\eta_3 + \tfrac{\alpha-1+\beta_t}{\beta_t}\eta_4\right)P_{t,\mathrm{h}}^{\mathrm{load,reai}}\right]
\end{aligned}
\tag{C1}
$$

The stationarity condition in KKT is:

$$
\begin{cases}
\frac{\partial L}{\partial P_{t,\mathrm{e}}^{\mathrm{load,reai}}} = p_{t,\mathrm{e}}^{\mathrm{opt}} - \left[\frac{1-\alpha}{\beta_t}\eta_3 + \frac{\alpha-(1-\beta_t)}{\beta_t}\eta_4\right]\lambda_t^1 = 0 \\
\frac{\partial L}{\partial P_{\mathrm{t,h}}^{\mathrm{load,reai}}} = p_{t,\mathrm{h}}^{\mathrm{opt}} - \left[\frac{1-\alpha}{\beta_t}\eta_3 + \frac{\alpha-(1-\beta_t)}{\beta_t}\eta_4\right]\lambda_t^2 = 0 \\
\frac{\partial L}{\partial P_{t,\mathrm{e}}^{\mathrm{cut}}} = f_{t,\mathrm{e}}^{\mathrm{cut}} - \mu_t^1 + \mu_t^2 - \lambda_t^1 = 0 \\
\frac{\partial L}{\partial P_{t,\mathrm{h}}^{\mathrm{cut}}} = f_{t,\mathrm{h}}^{\mathrm{cut}} - \mu_t^3 + \mu_t^4 - \lambda_t^2 = 0 \\
\frac{\partial L}{\partial P_{c,\mathrm{pv}}^{\mathrm{DPP,real}}} = -f_{\mathrm{pv}}^{\mathrm{dis}} - \mu_t^5 + \mu_t^6 \\
-[(2-2\alpha)\eta_2 + (2\alpha-1)\eta_1]\lambda_t^2 = 0
\end{cases}
\tag{C2}
$$

The complementary relaxation condition is:

$$
\begin{cases}
0 \le \left(P_{t,\mathrm{e}}^{\mathrm{cut}} - P_{\mathrm{min,e}}^{\mathrm{cut}}\right) \perp \mu_t^1 \ge 0 \\
0 \le \left(P_{\mathrm{max,e}}^{\mathrm{cut}} - P_{t,\mathrm{e}}^{\mathrm{cut}}\right) \perp \mu_t^2 \ge 0 \\
0 \le \left(P_{t,\mathrm{h}}^{\mathrm{cut}} - P_{\mathrm{min,h}}^{\mathrm{cut}}\right) \perp \mu_t^3 \ge 0 \\
0 \le \left(P_{\mathrm{max,h}}^{\mathrm{cut}} - P_{t,\mathrm{h}}^{\mathrm{cut}}\right) \perp \mu_t^4 \ge 0 \\
0 \le \left(P_{t,\mathrm{pv}}^{\mathrm{PVP,real}}\right) \perp \mu_t^5 \ge 0 \\
0 \le \left(P_{t,\mathrm{pv}}^{\mathrm{PVP}} - P_{t,\mathrm{pv}}^{\mathrm{PVP,real}}\right) \perp \mu_t^6 \ge 0
\end{cases}
\tag{C3}
$$

The complementary relaxation conditions are linearized by using the large M method.

$$
\begin{cases}
0 \le P_{t,\mathrm{e}}^{\mathrm{cut}} - P_{\mathrm{min,e}}^{\mathrm{cut}} \le \delta_t^1 M \\
0 \le \mu_t^1 \le (1-\delta_t^1)M
\end{cases}
\begin{cases}
0 \le P_{\mathrm{max},e}^{\mathrm{cut}} - P_{t,e}^{\mathrm{cut}} \le \delta_t^2 M \\
0 \le \mu_t^2 \le (1-\delta_t^2)M
\end{cases}
$$

$$
\begin{cases}
0 \le P_{t,\mathrm{h}}^{\mathrm{cut}} - P_{\mathrm{min},h}^{\mathrm{cut}} \le \delta_t^3 M \\
0 \le \mu_t^3 \le (1-\delta_t^3)M
\end{cases}
\begin{cases}
0 \le P_{\mathrm{max,h}}^{\mathrm{cut}} - P_{t,\mathrm{h}}^{\mathrm{cut}} \le \delta_t^4 M \\
0 \le \mu_t^4 \le (1-\delta_t^4)M
\end{cases}
\tag{C4}
$$

$$
\begin{cases}
0 \le P_{t,\mathrm{pv}}^{\mathrm{PVP,real}} \le \delta_t^5 M \\
0 \le \mu_t^5 \le (1-\delta_t^5)M
\end{cases}
\begin{cases}
0 \le P_{t,\mathrm{pv}}^{\mathrm{PVP}} - P_{t,\mathrm{pv}}^{\mathrm{PVP,real}} \le \delta_t^6 M \\
0 \le \mu_t^6 \le (1-\delta_t^6)M
\end{cases}
$$

where $\delta_t^1\delta_t^2\delta_t^3\delta_t^4\delta_t^5\delta_t^6$ are the introduced Boolean variable used for linearization expression, and M is a sufficiently large positive number, which is taken as 10^8 in this paper.

Through the above derivation, by replacing the original follower problem with Eqs. (C1) and (C2), the equivalent single-layer form of the double-layer optimization can be obtained.

Then, considering the bilinear term in the objective function, which is the product of the electricity-heat price and the electricity-heat purchase quantity ($P_t^{\mathrm{opt}}P_{t,\mathrm{h}}^{\mathrm{load,reai}}$ and $P_{t,\mathrm{h}}^{\mathrm{opt}}P_{t,\mathrm{h}}^{\mathrm{real,load}}$), the strong duality method is adopted for linearization processing.

In order to obtain the explicit expression of the dual problem, taking the partial derivatives of $P_{t,\mathrm{e}}^{\mathrm{load,reai}}$ and $P_{t,\mathrm{h}}^{\mathrm{load,reai}}$ setting them to zero, we can obtain:

$$
\begin{aligned}
&\frac{\partial L}{\partial P_{t,\mathrm{e}}^{\mathrm{load,reai}}} = p_{t,\mathrm{e}}^{\mathrm{opt}} - \left[\frac{1-\alpha}{\beta_t}\eta_3 + \frac{\alpha-(1-\beta_t)}{\beta_t}\eta_4\right]\lambda_t^1 = 0 \\
&\frac{\partial L}{\partial P_{t,\mathrm{h}}^{\mathrm{load,reai}}} = \mathrm{p}_{t,\mathrm{h}}^{\mathrm{opt}} - \left[\frac{1-\alpha}{\beta_t}\eta_3 + \frac{\alpha-(1-\beta_t)}{\beta_t}\eta_4\right]\lambda_t^2 = 0
\end{aligned}
\tag{C5}
$$

After simplification, we obtain:

$$
\begin{aligned}
p_{t,\mathrm{e}}^{\mathrm{opt}} &= \lambda_t^1\left[\frac{\beta_t}{(1-\alpha)\eta_3} + \frac{\beta_t}{(\alpha-1+\beta_t)\eta_4}\right] \\
p_{t,\mathrm{h}}^{\mathrm{opt}} &= \lambda_t^2\left[\frac{\beta_t}{(1-\alpha)\eta_3} + \frac{\beta_t}{(\alpha-1+\beta_t)\eta_4}\right]
\end{aligned}
\tag{C6}
$$

According to the strong duality theory, the optimal value of the original problem is equal to that of the dual problem, and the optimization direction remains unchanged. Therefore, the bilinear variables are equivalent to:

$$
\begin{aligned}
&\sum_{t=1}^{T}\left(p_{t,\mathrm{e}}^{\mathrm{opt}}P_{t,\mathrm{e}}^{\mathrm{load,reai}} + p_{t,\mathrm{h}}^{\mathrm{opt}}P_{t,\mathrm{h}}^{\mathrm{load,reai}}\right) = \\
&\sum_{t=1}^{T}\left[P_{t,\mathrm{e}}^{\mathrm{load,reai}}\left(\lambda_t^1\left[\frac{\beta_t}{(1-\alpha)\eta_3} + \frac{\beta_t}{(\alpha-1+\beta_t)\eta_4}\right]\right) + P_{t,\mathrm{h}}^{\mathrm{load,reai}}\left(\lambda_t^2\left[\frac{\beta_t}{(1-\alpha)\eta_3} + \frac{\beta_t}{(\alpha-1+\beta_t)\eta_4}\right]\right)\right]
\end{aligned}
\tag{C7}
$$

In conclusion, the objective function and constraints of the single-layer model obtained after the equivalence of the double-layer model of VPPO and UA can be rewritten as:

$$
\begin{aligned}
&\min C_{\mathrm{VPP}} = f_{\mathrm{gas}}\sum_{t=1}^{T}\left(P_{t,\mathrm{gas}}^{\mathrm{CHP}} + P_{t,\mathrm{gas}}^{\mathrm{GB}}\right) + f_{\mathrm{ESS}}\sum_{t=1}^{T}P_t^{\mathrm{dis}} + \\
&f_{\mathrm{pv}}^{\mathrm{dis}}\sum_{t\in c}^{T}\left(P_{t,\mathrm{pv}}^{\mathrm{VPPO}} - P_{t,\mathrm{pv}}^{\mathrm{VPPO,real}}\right) + f_{\mathrm{wt}}^{\mathrm{dis}}\sum_{t\in c}^{T}\left(P_{t,\mathrm{wt}}^{\mathrm{VPPO}} - P_{t,\mathrm{wt}}^{\mathrm{VPPO,real}}\right) + \\
&\sum_{t=1}^{T}\left(p_{t,\mathrm{e}}^{\mathrm{buy}}P_{t,\mathrm{e}}^{\mathrm{buy}} - p_{t,\mathrm{e}}^{\mathrm{sell}}P_{t,\mathrm{e}}^{\mathrm{sell}}\right) \\
&\sum_{t=1}^{T}\left[P_{t,\mathrm{e}}^{\mathrm{load,reai}}\left(\lambda_t^1\left[\frac{\beta_t}{(1-\alpha)\eta_3} + \frac{\beta_t}{(\alpha-1+\beta_t)\eta_4}\right]\right) + P_{t,\mathrm{h}}^{\mathrm{load,reai}}\left(\lambda_t^2\left[\frac{\beta_t}{(1-\alpha)\eta_3} + \frac{\beta_t}{(\alpha-1+\beta_t)\eta_4}\right]\right)\right] \\
&s.t.\begin{cases}(2)-(6),(9)-(10),(17)-(20), \\ (B3),(C2),(C4),(C7)\end{cases}
\end{aligned}
\tag{C8}
$$

At this point, by applying the strong duality principle and eliminating the nonlinear term of the bilinear product through the KKT conditions, the Nash-Stackelberg model has been transformed into a single-layer mixed integer linear programming problem with the objective function (C8), which can be directly solved using a commercial solver such as Cplex.

Appendix D

When the Nash bargaining solution satisfies the four axiomatic conditions of Nash, it can be proved to be the optimal solution [25–27]. The specific proof process is as follows:

1 Pareto efficiency

Axiom requirement: The outcome of the bargaining must be at the Pareto frontier, meaning that there is no other feasible option that can increase the benefits of at least one party without harming the interests of any other party.

Proof. It is known that the local optimal solution of a single-objective convex optimization problem is the global optimal solution. The Nash bargaining model in this paper decomposes the cooperative game of multiple VPPs into two single-objective convex optimization problems through equivalent transformation:

SP1: The objective function is to minimize the total cost of the VPP alliance:

$$\max \prod_{i=1}^{3} \left(C_{\mathrm{VPP}i}^{\mathrm{non}} - C_{\mathrm{VPP}i}^{\mathrm{coo}}\right)^{\lambda_i} \tag{D3}$$

where, the objective function in the ADMM algorithm is decomposed into three independent linear functions. The linear functions are special convex functions, so SP1 belongs to single-objective convex optimization, and its optimal solution must fall on the Pareto front, with no Pareto improvement space.

SP2: With the objective of maximizing the revenue distribution of the VPP alliance

$$\min \sum_{i=1}^{3} -\ln\left[C_{\mathrm{VPP}i}^{\mathrm{non}} - \left(C_{\mathrm{VPP}i}^{\mathrm{coo}} + C_{\mathrm{VPP}i}^{\mathrm{p2p}}\right)\right] \tag{D4}$$

where, the objective function in the ADMM algorithm is decomposed into three independent natural logarithms. Since the natural logarithm is a strictly monotonically increasing convex function, its optimal solution has a higher benefit after the cooperation of all VPPs than the benefit of independent operation. It cannot be improved by Pareto and ultimately falls on the Pareto frontier.

Therefore, it can be proved that the optimal solutions of SP1 and SP2 in this paper satisfy Pareto optimality, and thus the results of the entire Nash bargaining model comply with the requirements of Pareto optimality.

2 Symmetry

Axiom requirement: If the positions of all the negotiating parties are completely symmetrical, then the bargaining outcome should also be symmetrical.

Proof. This paper considers the standard Nash bargaining model, where it is assumed that all VPPs have the same bargaining position, that is, λ_i are all equal to 1, and the objective function is:

$$\max \prod_{i=1}^{3} \left(C_{\mathrm{VPP}i}^{\mathrm{non}} - C_{\mathrm{VPP}i}^{\mathrm{coo}}\right)^{\lambda_i} \tag{D5}$$

On the other hand, the ADMM distributed solution process in Section 3.2 shows that the interaction power among the entities is inversely proportional, as shown in Eq. (29); the interaction prices are the same, as shown in Eq. (31). This further verifies the requirement for symmetry. Therefore, the information exchange rules among all VPPs and the update formulas for Lagrange multipliers are unified for all VPPs, and the bargaining positions of each VPP are the same.

3 Invariance to affine transformations

Axiom requirement: Applying a positive affine transformation to the utility increment of any VPP will not change the bargaining outcome.

Proof. This paper considers the standard Nash bargaining model, and the objective function to be optimized is:

$$\max \prod_{i=1}^{3} \left(C_{\mathrm{VPP}i}^{\mathrm{non}} - C_{\mathrm{VPP}i}^{\mathrm{coo}}\right)^{\lambda_i} \tag{D6}$$

Let k be the positive affine transformation coefficient ($k > 0$), and the transformed Nash bargaining objective is to maximize the product of the transformed utility increments:

$$\begin{aligned} &\max \prod_{i=1}^{3} \left(k \cdot C_{\mathrm{VPP}i}^{\mathrm{non}} - k \cdot C_{\mathrm{VPP}i}^{\mathrm{coo}}\right)^{\lambda_i} \\ &\Rightarrow \max \prod_{i=1}^{3} k^{\lambda_i} \prod_{i=1}^{3} \left(C_{\mathrm{VPP}i}^{\mathrm{non}} - C_{\mathrm{VPP}i}^{\mathrm{coo}}\right)^{\lambda_i} \end{aligned} \tag{D7}$$

where, since $\prod_{i=1}^{3} k^{\lambda_i}$ is a constant, the transformed Nash bargaining objective function is exactly in the same optimization direction as the original bargaining objective function. That is, maximizing the original function is equivalent to maximizing the transformed function. Therefore, the optimal solution satisfies the affine transformation invariance.

4 Independence of irrelevant alternatives

Axiom requirement: If certain unselected allocation schemes are removed from the feasible set, the bargaining solution should not change.

Proof. In this model, the bargaining solution is calculated by maximizing the cooperative benefits. This solution only depends on the boundary of the feasible set, namely the Pareto front. Removing internal points will not affect the optimality of the solution.

In conclusion, the optimal solution of the Nash bargaining model in this paper strictly satisfies the four axioms of Nash bargaining: Pareto efficiency, Symmetry, Invariance to affine transformations, and Independence of irrelevant alternatives.

Appendix E

The demand for electric heating load and the prediction of wind and solar power are shown in Fig. E1-E4.

Fig. E1. PVP electric load requirements

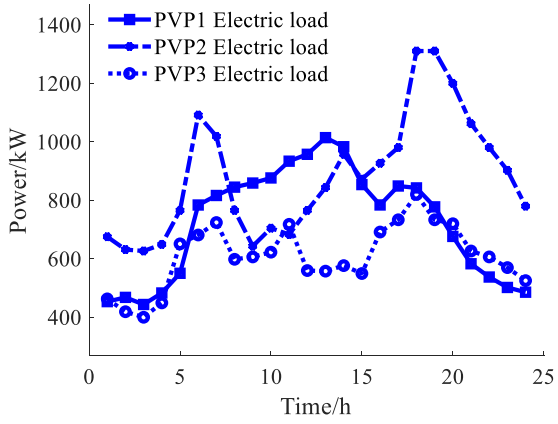

Fig. E2. PVP heating load requirements

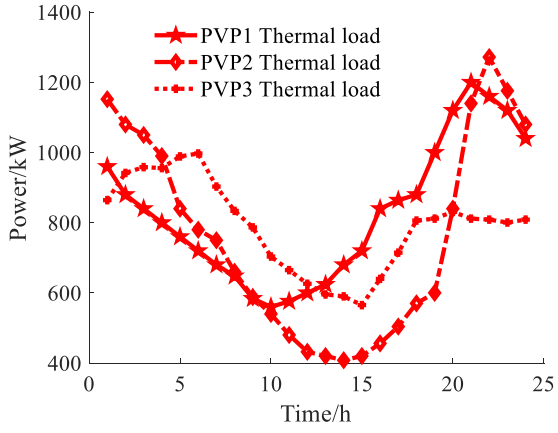

Fig. E3. Wind and Solar power Prediction of VPPO

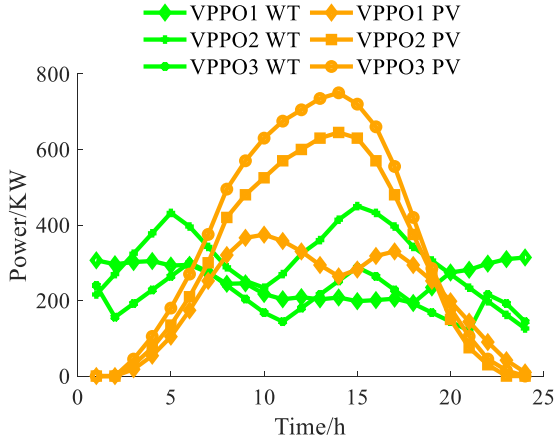

Fig. E4. PVP Photovoltaic Power Prediction

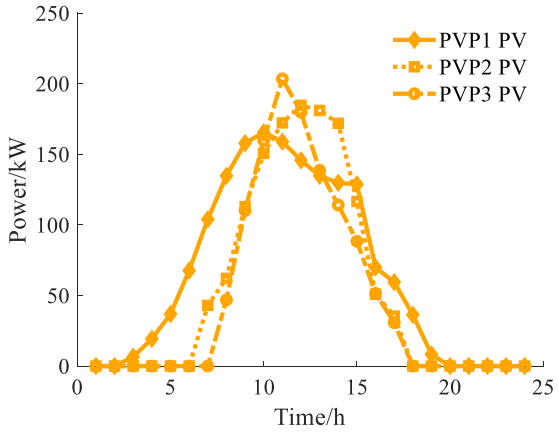

The time-of-use electricity price and time-of-use heat price for external transactions are shown in Fig. E5-E6.

Fig. E5. Time-of-use Electricity Price

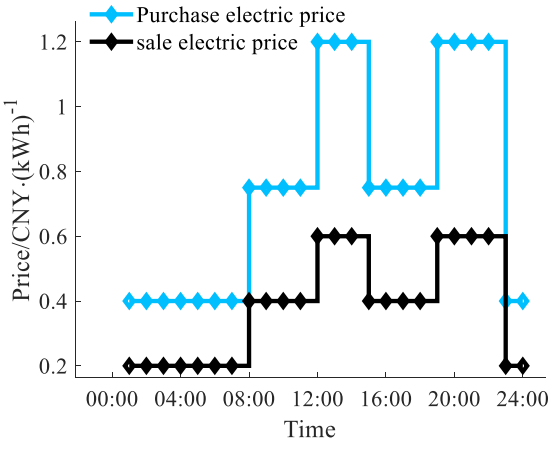

Fig. E6. Time-of-use thermal Price

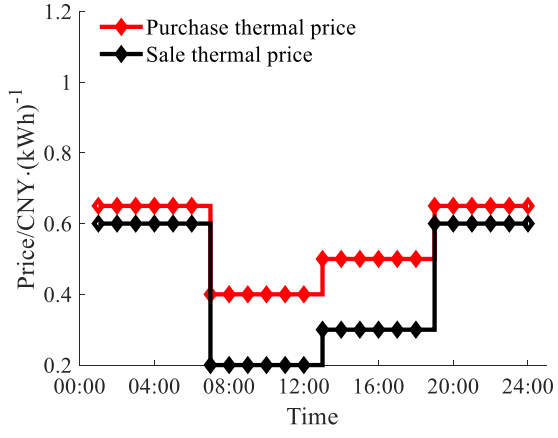

The Settings of operation parameters and cost parameters are shown in Table E1.

Table E1
Parameter settings.

Parameters	Numerical value	Unit
θ_{e}^{CHP}	45	%
Q_{gas}	8.4×10^{7}	J/m^3
$P_{min,e}^{CHP} P_{max,e}^{CHP}$	0,800	kW/h
$P_{min,h}^{CHP} P_{max,h}^{CHP}$	0,800	kW/h
θ_{h}^{GB}	90	%
$P_{min,h}^{GB} P_{max,h}^{GB}$	0,500	kW/h
ϕ	25	%
$P_{cl,chr}^{min} P_{cl,dis}^{min} P_{cl,chr}^{max} P_{cl,dis}^{max}$	0,0,40,60	kW/h
$P_{e,buy}^{max} P_{e,sell}^{max} P_{h,buy}^{max} P_{h,sell}^{max}$	500,300,800,500	kW/h
f_{gas}	2.7	CNY/m^{-3}
f_{ESS}	0.2	CNY /kWh
f_{dis}	0.5	CNY /kWh
$f_{t}^{DR} f_{t,e}^{cut} f_{t,h}^{cut}$	0.5	CNY /kWh

References

[1] C. Tan, Z. Tan, G. Wang, et al., Business model of virtual power plant considering uncertainty and different levels of market maturity[J], J. Clean. Prod. 362 (2022) 131433.

[2] S. Feng, H. Ren, W. Zhou, A review of uncertain factors and analytic methods in long-term energy system optimization models [J], Global Energy Interconnect. 6 (04) (2023) 450–466.

[3] Q. Lu, L. Chen, S. Mei, Typical applications and prospects of game theory in power system [J], Proc. CSEE 34 (29) (2014) 5009–5017.

[4] L. Dong, S. Tu, L.I. Ye, et al., A stackelberg game model for dynamic pricing and energy management of multiple virtual power plants using metamodel-based optimization method [J], Power Syst. Technol. 44 (03) (2020) 973–983.

[5] J. Zhong, Y. Zhao, Y. Li, et al., Synergistic operation framework for the energy hub merging stochastic distributionally robust chance-constrained optimization and Stackelberg game[J], IEEE Trans. Smart Grid 16 (2) (2024) 1037–1050.

[6] J. Wang, X. Jin, H. Jia, et al., Joint electricity and carbon sharing with PV and energy storage: a low-carbon DR-based game theoretic approach [J], IEEE Trans. Sustainable Energy 15 (4) (2024) 2703–2717.

[7] W. Huo, Y. Zhang, H. Zhao, et al., Wind power data pricing method based on an alliance cooperation game [J], Power Syst. Protect. Contr. 52 (19) (2024) 97–107.

[8] J. Wu, P. Lou, M. Guan, et al., Operation optimization strategy of multi-microgrids energy sharing based on asymmetric nash bargaining[J], Power Syst. Technol. 46 (07) (2022) 2711–2723.

[9] H. Rong, H. Kuang, A cooperative model of photovoltaic and electricity-to-hydrogen including green certificate trading under the conditional value at risk[J], Global Energ. Int. 6 (04) (2023) 403–417.

[10] X. Liu, Bi-layer game method for scheduling of virtual power plant with multiple regional integrated energy systems [J], Int. J. Electr. Power Energy Syst. 149 (2023) 109063.

[11] Y. Cao, D. Wang, H. Jia, et al., Bilevel Nash-Stackelberg game expansion planning of regional integrated energy system considering multi-energy carbon flow constraints [J], Automat. Electr. Power Syst. 47 (07) (2023) 12–22.

[12] J. Tan, Y. Li, X. Zhang, et al., Operation of a commercial district integrated energy system considering dynamic integrated demand response: a Stackelberg game approach [J], Energy 274 (2023) 126888.

[13] Y. Zhu, Y. Xiao, X. Wang, et al., Enhancing distribution system resilience with peer-to-peer transactions [J], IEEE Trans. Power Syst. 40 (1) (2025) 907–919.

[14] Y. Shi, H. Wang, C. Li, et al., Stochastic optimization of system configurations and operation of hybrid cascade hydro-wind-photovoltaic with battery for uncertain medium-and long-term load growth [J], Appl. Energy 364 (2024) 123127.

[15] F. Fang, S. Yu, X. Xin, Data-driven-based stochastic robust optimization for a virtual power plant with multiple uncertainties [J], IEEE Trans. Power Syst. 37 (1) (2021) 456–466.

[16] S. Wu, X. Qi, X. Li, et al., Collaborative robust dispatch of electricity and carbon under carbon allowance trading market [J], Global Energy Interconnect. 7 (04) (2024) 391–401.

[17] S. Liu, Q. Ai, J. Zheng, et al., Bi-level coordination mechanism and operation strategy of multi-time scale multiple virtual power plants [J], Proc. CSEE 38 (03) (2018) 753–761.

[18] Y. Lin, S. Miao, W. Yang, et al., J. Global Energ. Interconn. [J]. 5 (02) (2022) 127–137.

[19] Y. Lin, S. Miao, W. Yang, et al., Day-ahead optimal scheduling strategy of virtual power plant for environment with multiple uncertainties [J], Electr. Power Automat. Equip. 41 (12) (2021) 143–150.

[20] W. Zhong, S. Huang, C.U.I. Yang, et al., W-S-C capture coordination in virtual power plant considering source-load uncertainty [J], Power Syst. Technol. 44 (09) (2020) 3424–3432.

[21] R. Liu, Y. Liu, Z. Jing, Impact of industrial virtual power plant on renewable energy integration [J], Global Energy Interconnect. 3 (06) (2020) 545–552.

[22] M. Song, G. Lin, G.A.O. Ci, et al., A generalized shared energy storage optimization configuration method considering multiple uncertainties [J], Trans. China Electrotechn. Soc. 40 (05) (2025) 1521–1539.

[23] L. Dong, Y. Li, S. Chen, et al., Multi-microgrid cooperative game optimization scheduling considering multiple uncertainties and coupled electricity-carbon transactions[J], Trans. China Electrotechn. Soc. 39 (09) (2024) 2635–2651.

[24] Z. Wang, H. Hou, B. Zhao, et al., Risk-averse stochastic capacity planning and P2P trading collaborative optimization for multi-energy microgrids considering carbon emission limitations: an asymmetric Nash bargaining approach [J], Appl. Energy 357 (2024) 122505.

[25] Y. Jia, C. Wan, W. Cui, et al., Peer-to-peer energy trading using prediction intervals of renewable energy generation[J], IEEE Trans. Sustain. Smart Grid 14 (2) (2023) 1454–1465.

[26] H.K. Nguyen, A. Khodaei, Z. Han, Incentive mechanism design for integrated microgrids in peak ramp minimization problem, [J], IEEE Trans. Sustain. Smart Grid 9 (6) (2018) 5774–5785.

[27] S. Fan, Q. Ai, L. Piao, Bargaining-based cooperative energy trading for distribution company and demand response [J], Appl. Energy 226 (2018) 469–482.

[28] B. He, X. Yuan, A class of admm-based algorithms for three-block separable convex programming [J], Comput. Optim. Appl. 70 (3) (2018) 791–826.

[29] J. Zhang, L. Che, X. Wan, et al., Distributed hierarchical coordination of networked charging stations based on peer-to-peer trading and EV charging flexibility quantification [J], IEEE Trans. Power Syst. 37 (4) (2021) 2961–2975.

[30] D. Yan, Y. Chen, Distributed coordination of charging stations with shared energy storage in a distribution network [J], IEEE Trans. Smart Grid 14 (6) (2023) 4666–4682.

[31] T. Zhang, T. Pu, L. Dong, et al., Distributed reactive power optimization for flexible distribution networks with successive relaxation iteration method [J], IEEE Trans. Sustain. Energy 16 (1) (2024) 452–468.
[32] A. Mansour-Saatloo, Y. Pezhmani, M.A. Mirzaei, et al., Robust decentralized optimization of multi-microgrids integrated with power-to-X technologies [J], Appl. Energy 304 (2021) 117635.
[33] L. Chen, S. He, X. Fan, Cooperative optimization of shared energy storage in integrated energy systems using adaptive ADMM and Nash bargaining [J], J. Storage Mater. 134 (2025) 118148.

Lei Dong, professor of North China Electric Power University, doctoral supervisor. Her research directions include optimal dispatching and operation control of power grids, optimization of integrated energy systems, and the application of artificial intelligence in power systems, etc.